Sorption and Permeation of Gases in Hyper-Cross-Linked Hybrid Poly(POSS-imide) Networks: An in silico Study

David Brown, Sylvie Neyertz, Michiel J.T. Raaijmakers, Nieck Benes

Version of Record: https://www.sciencedirect.com/science/article/pii/S0376738818329843
Manuscript_3622e938af2aa867f4e1291210f1f0d2

Sorption and Permeation of Gases in Hyper-Cross-Linked Hybrid Poly(POSS-imide) Networks: An *in silico* Study

David Brown*[a], Sylvie Neyertz [a], Michiel J. T. Raaijmakers[b,c] and Nieck E. Benes[b]

[a]University Savoie Mont Blanc, CNRS, G-INP[†], LEPMI, F-73000 Chambéry, France

[†]Institute of Engineering, University Grenoble Alpes

[b]Membrane Science and Technology Cluster, University of Twente, The Netherlands

[c]Current address: AkzoNobel Chemicals B. V., Zutphenseweg 10, 7418 AJ Deventer, P.O. Box 10, 7400 AA Deventer, The Netherlands

[*]Corresponding Author: E-mail: David.Brown@univ-smb.fr

Abstract

Networked hybrid materials containing various types of organic imides covalently bonded with polyhedral oligomeric silsesquioxanes (POSS) have recently been developed. One of their possible applications is for gas-separation under extreme conditions of pressure and/or temperature. Experimental results indicate that their permeation properties depend on the specific organic dianhydride precursor used in the synthesis. In this work, atomistic models of 6FDA-based and PMDA-based poly(POSS-imide) crosslinked networks have been used to investigate the sorption, desorption, relaxation and permeation properties of such materials at the molecular level and their dependence on the nature of the imide linker. Results have been compared to available experimental data.

A highly-efficient parallelised version of the excluded volume map sampling test particle insertion (EVMS-TPI) method was used to obtain the infinite dilution solubilities of a number of small penetrants (N_2, O_2, CH_4 and CO_2) in these model networks. Analyses of the Boltzmann-weighted probability densities for the distribution of the insertion energies showed that very reliable estimates of solubilities could be obtained.

Extensive molecular dynamics simulations were then performed to obtain the complete model sorption isotherms for CO_2 and CH_4 at 35°C up to pressures of over 60 bar using an iterative technique which matches the chemical potential of the penetrant in the poly(POSS-imide) phase to that in the corresponding gas phase. The sorption-induced changes in volume, the significant space available to penetrants, the mean insertion energies and their distributions were characterized. Comparisons were not only made between both types of poly(POSS-imide) to characterize the effect of the linker, but also with (hypothetical) uncrosslinked mixtures of the POSS and dianhydride molecules in order to elucidate the

effects of crosslinking. Given the known conditioning properties of CO_2, desorption isotherms were also obtained for this penetrant. These showed significant hysteresis. Prolonged exposure to high concentrations of CO_2 was also found to lead to slow relaxations that have significant effects on the solubility.

Permeabilities were obtained for methane and carbon dioxide at 100°C, 200°C and 300°C at a pressure of ~2 bar. Differences in permeabilities were largely diffusion dependent.

Keywords: molecular dynamics (MD) simulations; 6FDA and PMDA poly(POSS-imide) networks; carbon dioxide and methane sorption, diffusion and permeation.

1. Introduction

The class of networked hybrid materials formed from polyhedral oligomeric silsesquioxanes (POSS), of basic formula $(RSiO_{3/2})_n$, with organic bridges [1-8] has recently received renewed interest in the case where the organic linker is an imide [9-13]. These materials combine the mechanical rigidity of inorganic siloxane cages [14], which act as the nodal centres in the networks, with flexible yet chemically stable organic imide moieties [15]. The latter are covalently bonded to the corners of the siloxane cages and thus form bridging links which give the networks their structural integrity. The actual synthesis of these poly(POSS-imide)s [9-13] passes first by an interfacial polymerization step, where an aqueous solution of a primary amine-functionalized POSS enters into contact with a solution of the dianhydride (corresponding to the target imide) dissolved in an organic solvent. A polycondensation reaction rapidly occurs at the interface between the two immiscible solutions, leading to the formation of a homogeneous film of the corresponding poly(POSS-(amic acid)). The films that are formed are relatively thin since the progressive formation of the dense film at the interface ultimately prevents further reactants from coming into contact [16]. The second stage of the synthesis involves heating the film to temperatures of ~300°C so as to convert the amic acid groups into cyclic imide groups. The relative simplicity of the approach lends itself, in principle, to industrial production of membrane films of arbitrary width and length [16].

One of the potential applications of poly(POSS-imide) membranes is in the field of gas separations under conditions of high pressures and/or temperatures [9], where the added stability of the inorganic/organic network offers advantages over uncrosslinked glassy polyimides. Indeed, the latter can have their separation performances affected by increased mobility or plasticization [17], e.g. at high temperatures and/or by highly soluble penetrants, such as CO_2. The large variety in the choice of the imide bridges gives a certain control over the inter-cage spacing and link flexibility [10] and this in turn affects the transport, which is known to occur uniquely in the organic phase [18]. For example, the permeances of various gases were found to increase with the imide bridge length, whereas selectivities for

different gas pairs tended to decrease [10]. In addition, it has also been shown that the imide to POSS ratio can be controlled to a certain extent by changing the POSS concentration in the aqueous solution [13]. This latter study demonstrated that the sorption and swelling behaviour induced by penetrants such as carbon dioxide and methane is likely to be very sensitive to the imide to POSS ratio.

To provide complementary insights into the way that various linkers [5] affect the structure and dynamics of poly(POSS-imide)s, we have recently constructed detailed atomistic bulk models of such networks by *in silico* polymerization of equilibrated mixtures of $(NH_2\text{-}(CH_2)_3\text{-}SiO_{3/2})_8$ with two different imide linkers [19, 20]: (a) the pyromellitic dianhydride (PMDA), a short and fairly rigid linker, and (b) the 4,4'-(hexafluoroisopropylidene) diphthalic dianhydride (6FDA), a longer and more flexible linker. Their chemical structures are sketched in Fig. 1.

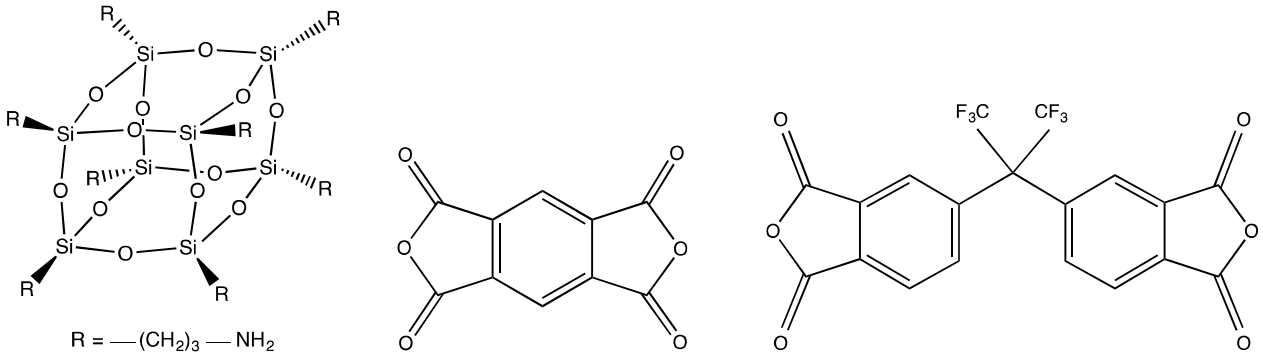

POSS **PMDA dianhydride** **6FDA dianhydride**

Figure 1. Chemical structures of the octa(aminopropylsilsesquioxane) POSS, the PMDA dianhydride and the 6FDA dianhydride precursors.

In order to mimick the experimental synthesis, the model polymerization produced intermediate poly(POSS-(amic acid)) systems, which were converted to their poly(POSS-imide) forms at high temperature. The resulting bulk poly(POSS-imide) networks were extensively simulated using classical molecular dynamics (MD) simulations and their structural, thermal and mechanical properties were characterized for both linkers under study at the same cross-linking density [19, 20]. A number of interesting insights were gained from these comparisons as well as detailed information concerning the cross-linking that is difficult to determine experimentally. For example, the interconnectivity of the POSS nodes was found to be rather heterogeneous with cages having the possibility, albeit low, of having all eight or none of their arms connected to other POSS cages, in spite of the average number of links per POSS being fixed at an experimentally-determined value of four [13]. The occurence of intramolecular links and multiple links between neighbouring POSS was also revealed as ~55% of cages had interPOSS single links only.

In terms of their use as gas separation membranes, the effect of the steric constraints introduced by network formation was clearly seen in the densities of the intermediate poly(POSS-(amic acid))s and final poly(POSS-imide)s decreasing with respect to that for an ideal mixture, thus revealing the creation of additional free-volume. Significantly, this effect was more pronounced in the case of the stiffer shorter PMDA linker.

The main objective here is to compare the gas sorption and permeation in the PMDA and 6FDA poly(POSS-imide)s models prepared previously. Calculations of infinite dilution solubilities of different small penetrants relevant to gas separations (N_2, O_2, CH_4 and CO_2) were first made at 35°C, 100°C, 200°C and 300°C. Extensive MD simulations were then performed to obtain the complete sorption curves for carbon dioxide and methane at 35°C up to pressures of over 60 bar using an iterative technique [21]. The method matches the chemical potential of the penetrant in the poly(POSS-imide) phase to that in the corresponding gas phase. In the case of carbon dioxide, the desorption curve was also calculated given its known conditioning properties, i.e. the irreversible sorption-induced relaxations that occur above a critical amount of volume dilation [13, 22].

Another objective was to evaluate the effect of the cross-linking procedure on gas sorption. For this reason, the infinite dilution solubility tests and the complete uptake curves of CO_2 and CH_4 at 35°C were also made on the corresponding 2:1 dianhydride+POSS uncrosslinked mixtures.

Finally, as the diffusion of the penetrants is rather limited at 35°C on the MD time scale, estimates of permeabilities were obtained for methane and carbon dioxide at the higher temperatures of 100°C, 200°C and 300°C for a pressure of ~2 bar. Experimentally, it has been found that short and stiff linkers, such as PMDA, show similar apparent activation energies for the permeation of several gases [10], whereas longer more flexible linkers, such as 6FDA, tend to give a range of apparent gas activation energies [9]. This leads to gas permselectivities varying significantly, and a better understanding is necessary so that these new materials can be optimized for specific gas separation applications. Whenever possible, the results were compared to the available experimental evidence.

2. Models and methods

All details concerning the fully-atomistic models of the octa(aminopropylsilsesquioxane) POSS, PMDA dianhydride and 6FDA dianhydride molecules as well as the intermediate poly(POSS-(amic acid))s and resulting poly(POSS-imide)s have been given previously along with the basic parameters and techniques used in the MD simulations [19, 20]. In brief, all bonds are considered rigid and a classical force field is used to represent the bond-angle bending, dihedral angle rotations, sp^2 out-of-plane deformations, Van der Waals and Coulombic interactions. In addition, special constraints [23-25] are applied to remove the degrees of freedom of hydrogen atoms in -CH_2 and aromatic -CH groups. All

parameters used were taken from literature sources [26-32] apart from the partial charges on each atom which were obtained using the Density Functional Theory calculations on representative fragments of the molecules [19, 20].

It should be pointed out that the model poly(POSS-imide)s are necessarily idealized in that some simplifications have been made [19, 20]. For example, the POSS cages are all considered to be T8, i.e. they contain 8 tetrahedral Si atoms, and all cages are kept intact whereas, in reality, they can be opened by partial hydrolysis to form silanol and SiO^- groups and recondensed [10-12, 33]. The ratio of linkers to POSS is kept constant at exactly 2:1 so as to maintain a constant imide:POSS ratio of 4:1 (each linker having an imide group at either end), thus the *average* number of links per POSS cage is automatically set to 4. Experimentally, this number is not straightforward to obtain with any precision and only rough estimates can be obtained from X-ray photoelectron spectroscopy (XPS) measurements [13]. It has been shown [10, 12] that, as far as can been determined, the linkers are indeed connected to a POSS cage at either end, i.e. there are no detectable dangling ends. However, the models of the pure bulk poly(POSS-imide)s are also completely free from any residual solvent molecules and ions, which is more difficult to achieve in reality. Apart from practical considerations, the advantage of adopting such simplifications in the models is that the comparison of the effects of the different linkers is less ambiguous.

2.1. Molecular dynamics simulations

The MD simulations were carried out using the domain decomposition parallelized code *ddgmq* [23] running on up to 27 processors. The equations of motion were solved using a leap-frog algorithm [34] and a time step of 1 fs. All rigid constraints were converged to within a relative tolerance of 10^{-6} using iterative techniques [24, 25]. The Ewald summation [35, 36] was used to calculate the Coulombic interactions and forces with parameters optimised in the manner described previously [23, 37, 38]. Van der Waals interactions were truncated at the same distance (typically 10 to 12 Å) as the real space term in the Ewald potential. Standard long-range corrections were made to the energy and pressure [34].

In general production simulations were carried out under $N\boldsymbol{P}T$ conditions (constant number of atoms N, controlled pressure tensor $\boldsymbol{P}$, controlled temperature T), as described previously [19, 20]. As will be explained later, following the introduction of penetrant molecules, simulations were generally run under NVT (constant number of atoms N, constant volume V, controlled temperature T) conditions for an initial period of 100 ps to allow for thermal equilibration before switching to $N\boldsymbol{P}T$ conditions. Thermodynamic data were stored every 1 ps, whereas configurations were stored every 5 ps for post-analyses.

2.2. Pure dianhydride+POSS uncrosslinked mixtures and poly(POSS-imide)s

The starting point for the model PMDA+POSS mixtures, 6FDA+POSS mixtures, and the PMDA and 6FDA poly(POSS-imide)s are the relaxed configurations obtained previously at 22°C [19, 20], since most of the basic experimental characterizations having been carried out at room temperature. For the dianhydride+POSS uncrosslinked mixtures, just one configuration was used in both cases. These systems contained 432 dianhydride molecules and 216 POSS molecules, i.e. a dianhydride to POSS ratio of 2:1. This amounts to 32832 and 41040 atoms, respectively for PMDA and 6FDA. Relaxed configurations of the mixtures at 35°C and 1 bar were obtained by performing a 4 ns simulation under *NPT* conditions; at this temperature, these systems are in a solid glassy state. It is important to state that the dianhydride+POSS uncrosslinked mixtures are hypothetical systems since the real mixtures undergo the reactions that form the poly(POSS-(amic acid))s. However, they will be used to assess the effect of cross-linking.

For the poly(POSS-imide)s, the starting point for the simulations were also taken from those obtained previously using a progressive approach to the formation of the network [19, 20]. We briefly summarize the procedure here. Based on initial XPS measurements [13], the average number of imide links per POSS was set to four in the model networks, i.e. a stoichiometric 2:1 ratio of the dianhydrides to POSS precursors. To increase the linking possibilities, mixtures with an excess of dianhydride, *e.g.* a 3:1 ratio, were prepared by first equilibrating the mixtures at 227°C before cooling at a rate of -0.1°C/ps to 22°C and then relaxing for at least 2000 ps. The cross-linking procedure was carried out in a progressive way at 22°C to form, in a first stage, the intermediate polyPOSS-(amic acid) networks. At any one instant, only the most favourably-placed dianhydride molecules, i.e. those satisfying a critical distance criterion, were "reacted" with POSS molecules by opening the 5-member anhydride ring and forming a covalent bond between a POSS amine nitrogen and one of the two ketone carbons on the anhydride. The strain created by the formation of new covalent bonds was then relaxed away by a combination of energy minimization and MD before attempting new reaction steps. The process of reaction step followed by relaxation step continued until the required number (432) of dianhydrides had been reacted. Excess unreacted dianhydrides were discarded at this point, so that the all networks did contain the experimentally-determined 2:1 ratio of dianhydride to POSS. There then followed a period of at least 10000 ps of relaxation at 300°C before the poly(POSS(amic acid)) networks were transformed to the imide form. This happened through a condensation "reaction" of each amide group and its adjacent carboxylic acid group with the elimination of water. The resulting poly(POSS-imide)s were further relaxed at 300°C for at least 5000 ps before being cooled down to 22°C at a rate of -0.1°C/ps and allowed to relax.

In this work, three independent poly(POSS-imide) samples for both types of dianhydride created using a distance criterion ≤ 6 Å for the network formation step were used [19, 20] as the starting configurations. The samples were first relaxed for 4 ns under ***NPT*** conditions at 35°C and 1 bar. Relaxed samples at 100°C were then obtained in the same way from the relaxed 35°C configurations and samples at 200°C were similarly obtained from those at 100°C. Samples at 300°C were taken from the original relaxations of the poly(POSS-imide)s at this temperature [19, 20].

2.3. Models of gases

Although four different gases (N_2, O_2, CH_4 and CO_2) were used as virtual penetrants in order to obtain estimations of their infinite dilution solubilities, specific gas+network and gas+mixtures MD simulations were only carried out for methane and carbon dioxide. All gas molecules were considered rigid to avoid problems of equipartition of energy due to either high-frequency low-amplitude vibrations or low moments of inertia. The diatomic molecules N_2 and O_2 were modelled using the two-centre point-quadrupole models of Vrabec *et al.* [39] and Hansen *et al.* [40], respectively. For CH_4 the 5-site model of Yin and Mackerell [41] was used albeit within the rigid tetrahedral representation described previously [42]. The model used for CO_2 was taken from the work of Zhang and Duan [43] as described in detail previously [44].

2.4. MD simulations of methane and carbon dioxide in the gas phase

As will be explained in the next section, it is necessary to know for the gas models the equilibrium pressure, number density or concentration, $C=n/V$ with n being the number of gas molecules and V the volume of the system, as well as the solubility, S, of the vapour phase along the isotherms at the different temperatures of interest (35°C, 100°C, 200°C and 300°C) in order to calculate the sorption curves for CH_4 and CO_2 in the poly(POSS-imide)s and uncrosslinked mixtures. MD simulations were thus carried out for each penetrant on systems containing 512 molecules for 10000 ps under *NVT* conditions at a range of concentrations corresponding to pressures from ~0.5 bar up to ~100 bar, and at all four temperatures. The average results were extracted from the last 6000 ps for CO_2, and the last 8000 ps for CH_4. A standard test-particle insertion (TPI) method was used to obtain the solubilities in the gas phase [45]. Analytical functions having the correct ideal gas limits at low pressures [23] were then fitted to the data obtained at discrete points in order to have interpolations of $C_{gas}(p)$ and $S_{gas}(p)$ at any pressure within the fitted regime.

2.5. Iterative method for obtaining pure gas sorption isotherms

In real sorption experiments, a finite sample of material is exposed directly to progressively higher pressures of the gas and the difficulty is to determine the change in mass of the sample. In simulations of bulk materials with 3D periodic boundary conditions, it is *a priori* possible to load the systems with an arbitrary number of penetrants. However, the difficulty is now to determine the pressure of the gas phase that would have to be put in contact with the system in order to obtain the imposed loading. An efficient iterative method [21] has been used to calculate the sorption curves for gases in the poly(POSS-imide)s and dianhydride+POSS uncrosslinked mixtures. Details of the method have already appeared [23, 44], so only the salient points will be given here.

For a matrix such as those under study, once equilibrium has been established between the polymer phase containing the sorbed gas and the pure gas phase, the chemical potential of the gas in the polymer phase, μ_{pol}, and the gas in the gas phase, μ_{gas}, should be equal; for simplicity we will use henceforth the suffix "pol" to indicate the phase containing either the poly(POSS-imide) or the uncrosslinked mixture. In the case of rigid gas molecules, the equality of the chemical potentials in the two phases implies that the difference in *excess* chemical potentials of the penetrant molecules in the two phases, μ_{gas}^{ex} and μ_{pol}^{ex}, is related to their different concentrations in the corresponding phases [46]:

$$\Delta\mu^{ex} = \mu_{pol}^{ex} - \mu_{gas}^{ex} = k_B T \ln \frac{C_{gas}}{C_{pol}} \tag{1}$$

A statistical mechanical approximation to the excess chemical potential, μ^{ex}, in the ***NPT*** ensemble is given by [47]:

$$\mu^{ex} = -k_B T \ln \frac{\left\langle V \exp\left(-\frac{\Delta\Phi}{k_B T}\right)\right\rangle}{\langle V \rangle} \tag{2}$$

where $\Delta\Phi$ is the potential energy change resulting from the virtual introduction of a penetrant molecule into configurations of the corresponding model. From Eq. 2, an expression for the (dimensionless) solubility is obtained:

$$S = \exp\left(\frac{-\mu^{ex}}{k_B T}\right) = \frac{\left\langle V \exp\left(-\frac{\Delta\Phi}{k_B T}\right)\right\rangle}{\langle V \rangle} \approx \left\langle \exp\left(-\frac{\Delta\Phi}{k_B T}\right)\right\rangle \tag{3}$$

the approximation in Eq. 3 being valid for dense materials where volume fluctuations are negligible.

Conventional TPI methods [45] use Eq. 3 to obtain solubilities by inserting the test particle at random positions. Although these methods work well at low densities, such as in the gas phase, they become rather inefficient at high densities since a favourable particle insertion at a randomly chosen position becomes increasingly unlikely. The excluded-volume map sampling (EVMS) approach [48-51] is much more efficient for dense systems as it pre-eliminates regions of very low insertion probabilities. Here a modified version [23, 44] of the EVMS TPI method was used via a parallel processing approach for accelerated sampling.

Equations 1, 2 and 3 can be combined to give a simple relationship between the ratios of the concentrations and solubilities for the penetrant in the two phases:

$$\frac{C_{gas}}{C_{pol}} = \exp\left(\frac{\Delta\mu^{ex}}{k_B T}\right) = \frac{\exp\left(\frac{-\mu_{gas}^{ex}}{k_B T}\right)}{\exp\left(\frac{-\mu_{pol}^{ex}}{k_B T}\right)} = \frac{S_{gas}}{S_{pol}} \quad \text{or alternatively} \quad \frac{C_{pol}}{C_{gas}} = \frac{S_{pol}}{S_{gas}} \tag{4}$$

This equation is used to determine the sorption isotherms. The simulations of the pure gas phase and their subsequent fits to analytical functions give interpolations for $C_{gas}(p)$ and $S_{gas}(p)$ at any pressure within the fitted regime. Then an MD simulation in the *NPT* ensemble is conducted for a matrix loaded with a given number of penetrants n_{pol}, at an initial (isotropic) required guess pressure p_1. This allows us to determine the average concentration of the gas in the polymer phase, $\langle C_{pol}(p_1)\rangle = n_{pol} / \langle V \rangle$, and the average solubility of the gas in the polymer phase, $\langle S_{pol}(p_1)\rangle$. The quantities $\langle C_{pol}(p_1)\rangle / C_{gas}(p)$ and $\langle S_{pol}(p_1)\rangle / S_{gas}(p)$ are plotted separately as a function of the variable pressure p of the gas phase and the point of intersection of the two curves provides the second approximation p_2. If this value is statistically different from p_1, another simulation of the gas in the matrix is conducted at a required pressure of p_2, and the process continues until convergence [21, 44].

At low pressures the intersection of the curves of relative density and relative solubility occur at angles close to perpendicular and the errors in the solubility of the gas in the polymer only lead to small errors in the iterated pressure. At higher pressures, the two curves become more tangential and thus errors in S_{pol} lead to larger errors in the iterated pressure.

2.6. Test particle insertion analyses of poly(POSS-imide)s and dianhydride+POSS uncrosslinked mixtures

The four gas models (Section 2.3) were used to obtain estimates of their infinite dilution solubilities in the pure poly(POSS-imide)s and the uncrosslinked mixtures at 35°C by performing EVMS

TPI analyses on the relaxed configurations. Averages were typically obtained over the last 1000 ps of the simulations. In addition, EVMS TPI analyses were also carried out on the pure poly(POSS-imide)s at the higher temperatures of 100°C, 200°C and 300°C.

To obtain solubility coefficients from the dimensionless solubilities (Eq. 3), we note first that the gas concentration *C(p)* in the polymer is generally given in terms of the "volume" of the gas absorbed, i.e. the hypothetical volume that the gas molecules in the matrix would occupy if they were an ideal gas at the standard temperature and pressure (STP) conditions, divided by the volume of the matrix:

$$C(p) = \frac{n_{pol}(p)}{V(p)} \cdot \frac{k_B T^{STP}}{p^{STP}} \tag{5}$$

where $n_{pol}(p)$ stands for the number of gas molecules absorbed in the matrix when in equilibrium with a gas phase at pressure p, T^{STP}=273.15 K and p^{STP}=1.01325 bar, respectively, and $V(p)$ is the volume of the matrix containing the absorbed gas. The solubility coefficient is then defined as:

$$S_c(p) = \frac{C(p)}{p} \tag{6}$$

By combining Eqs. 4, 5 and 6 it can be shown [44] that limiting values of the solubility coefficient for the matrices can be obtained from the infinite dilution solubilities, S_{pol}^0, i.e. the solubilities of the pure matrices before any penetrants have been added, using the following expression:

$$\lim_{p \to 0} S_c(p) = \frac{S_{pol}^0 T^{STP}}{T p^{STP}} \tag{7}$$

We mention in passing that although experimentally infinite dilution solubility coefficients are not directly accessible, they can be extrapolated from fits to sorption curves at non-zero pressures [61]. For example, a popular way of fitting the results of such experiments is the dual-mode sorption (DMS) model [62]:

$$C(p) = k_D p + C_H' \left(\frac{bp}{1+bp} \right) \quad \Rightarrow \quad S_c(p) = \frac{C(p)}{p} = k_D + C_H' \left(\frac{b}{1+bp} \right) \tag{8}$$

according to which gas sorption in glassy polymers occurs both by a "hole-filling" mechanism into the non-equilibrium excess volume associated with the glassy state (characterized by the Langmuir sorption capacity C_H' and the hole affinity b) and by a Henry's law dissolution into the dense regions (characterized by the constant k_D). In the limit of pressure tending to zero we obtain from Eq. 8 an extrapolation of the infinite dilution solubility coefficient:

$$\lim_{p\to 0} \; S_c(p) = k_D + C_H' b \tag{9}$$

Also calculated during the TPI analyses are the weighted mean test particle insertion energies, $\langle \Delta\Phi \rangle$, obtained from the following equation:

$$\langle \Delta\Phi \rangle = \frac{\left\langle \Delta\Phi * V \exp\left(-\frac{\Delta\Phi}{k_B T}\right)\right\rangle}{\left\langle V \exp\left(-\frac{\Delta\Phi}{k_B T}\right)\right\rangle} \tag{10}$$

The weighting by the Boltzmann factor ensures that these averages represent the typical mean interaction energies that the probe molecule would have if they were actually inserted into the matrices. The underlying histograms of raw insertion energies have also been accumulated with a resolution of $0.1 k_B T$ during the EVMS TPI analyses. These can be corrected for the bias implicit in EVMS and normalized to give the corresponding probability density distribution, $\rho(\Delta\Phi)$. This density distribution is related, in the case where volume fluctuations are small, to the solubility via:

$$S \approx \left\langle \exp\left(-\frac{\Delta\Phi}{k_B T}\right)\right\rangle = \int_{-\infty}^{+\infty} \rho(\Delta\Phi) \exp\left(-\frac{\Delta\Phi}{k_B T}\right) d\Delta\Phi \tag{11}$$

and to the mean insertion energy via:

$$\langle \Delta\Phi \rangle \approx \frac{\left\langle \Delta\Phi * \exp\left(-\frac{\Delta\Phi}{k_B T}\right)\right\rangle}{\left\langle \exp\left(-\frac{\Delta\Phi}{k_B T}\right)\right\rangle} = \frac{\int_{-\infty}^{+\infty} \Delta\Phi * \rho(\Delta\Phi) \exp\left(-\frac{\Delta\Phi}{k_B T}\right) d\Delta\Phi}{\int_{-\infty}^{+\infty} \rho(\Delta\Phi) \exp\left(-\frac{\Delta\Phi}{k_B T}\right) d\Delta\Phi} = \frac{\int_{-\infty}^{+\infty} \Delta\Phi * \rho_w(\Delta\Phi)\, d\Delta\Phi}{\int_{-\infty}^{+\infty} \rho_w(\Delta\Phi)\, d\Delta\Phi} \tag{12}$$

where we introduce the Boltzmann factor weighted probability density distribution for insertion energies:

$$\rho_w(\Delta\Phi) = \rho(\Delta\Phi) \exp\left(-\frac{\Delta\Phi}{k_B T}\right) \tag{13}$$

which gives an indication of the likely interaction energies that will occur for any probe molecule actually inserted into the matrices. The smoothness of $\rho_w(\Delta\Phi)$ depends very much on the quality of the unweighted distributions at low energies. Poorly-converged unweighted distributions will inevitably give rise to rather ragged weighted distributions when multiplied by the Boltzmann factor as this becomes

extremely large when $\Delta\Phi$ becomes more and more negative. This is a good test of the reliability of any TPI method, so this weighted distribution function is systematically inspected.

The third quantity obtained from the TPI analysis is a measure of the fraction of significant volume (*FSV*) that is responsible for 99.9% of the solubility. This approach thus uses an energetic criterion to estimate available volume rather than a simple geometric one [63-65]. The method exploits the fact that the integral in Eq. 11 converges relatively quickly to its plateau value as the Boltzmann factor rapidly diminishes when the insertion energy rises. The critical upper limit to the integral $\Delta\Phi_c$ that is required to obtain 99.9% convergence for the solubility is first determined and then the *FSV* is given by the integral of the unweighted distribution up to this critical value:

$$FSV = \int_{-\infty}^{\Delta\Phi_c} \rho\left(\Delta\Phi\right) d\Delta\Phi \tag{14}$$

This approach implicitly takes into account the specificity of each probe's interactions with the system and thus evaluates the significant volume that corresponds to the probe in question.

2.7. MD simulations of CO_2 and CH_4 in poly(POSS-imide)s and dianhydride+POSS uncrosslinked mixtures at 35°C

The calculations of the CO_2 and CH_4 sorption isotherms in the uncrosslinked mixtures and the poly(POSS-imide)s up to high pressures were initiated from each relaxed sample at 35°C, i.e. one sample each for the 2:1 mixtures and three samples each for the 6FDA and PMDA poly(POSS-imide)s. Rough estimates of a reasonable number of penetrants to add at the first step were obtained from the infinite dilution solubilities and Eq. 4. The loading at each successive step should be sufficiently large to provoke a measurable difference in the pressure without being too small as to require excessive computer time: for example, additions of 50 or 100 penetrants were used here in the case of the poly(POSS-imide)s.

To actually load the penetrants into the systems, the EVMS TPI technique was first used to locate the trial position of the penetrant with the lowest energy. A penetrant was then added at this position and the process repeated, taking into the account any added penetrants, until all the desired penetrants had been added. Such an approach eliminates the need to energy-minimize the system to alleviate any bad contacts.

Following loading, systems were simulated for 100 ps under *NVT* conditions in order to establish thermal equilibrium. They were then allowed to relax under ***NPT*** conditions for a further 1900 ps at the initial guess pressure p_1. As the error in the measured pressure in such MD simulations is typically ~1 bar,

the required pressure was set to 1 bar up until the point where loadings gave estimates of pressures in excess of 2 bar. At higher loadings, p_1 was either left at the value found at a previous loading or was estimated from extrapolations of points in the uptake curve at lower loadings.

After each change in the loading, the first 1000 ps were considered as a period of transition for the system to adjust and, in particular, for the volume to swell. As such, only the period from 1000 ps to 2000 ps was used to obtain the average properties and to determine the solubility of the penetrant in the matrix+gas system. As described in Section 2.5, the iterative method was then applied to find the second estimate of the pressure p_2, and if a further iteration was required, then another simulation of 1000 ps under *NPT* conditions was conducted at this new pressure. As relatively small changes in pressure do not change the density very much, the entire 1000 ps period was analysed for the second and higher iterations. The process continued until convergence.

To maintain a fairly constant rate of loading and improve the efficiency, systems at higher loadings were spawned from configurations of the systems at the preceding loading saved after 500 ps of relaxation [44]. Loading was continued up to pressures of at least 60 bar. In addition, the poly(POSS-imide)s simulations at the highest loading were extended to 20000 ps to check how sensitive the results are to the length of time exposed to a certain load; in real polymer membranes, ageing (albeit over times orders of magnitude longer) can have a significant effect on sorption and permeation [52-59], and such conditioning effects are even known to occur on the MD time scale [60]. Furthermore, as exposure to carbon dioxide at high pressures is known to lead to significant volume swelling and subsequent hysteresis upon desorption [13, 22], the poly(POSS-imide) systems containing CO_2 also had their desorption curves determined, using the reverse procedure to that for the uptake curves. Starting from the highest loaded systems relaxed for 20000 ps, a number of molecules were removed randomly from the system at each unloading step, and then an *NPT* simulation of 2000 ps was carried out. Again, just the period from 1000 to 2000 ps was used to obtain a second estimate of the pressure. If necessary, a second iteration was performed over a period of 1000 ps, and so forth as for the uptake curve. Once all the CO_2 had been removed, a period of 10000 ps was simulated in order to see the extent of any residual relaxation.

For the different independent samples of the same types of poly(POSS-imide), the results were averaged over the three samples containing the same number of penetrants.

2.8. MD simulations of CO_2 and CH_4 in poly(POSS-imide)s at 100°C, 200°C and 300°C

Permeation studies of several gases, including CO_2 and CH_4, have been carried out experimentally on the 6FDA poly(POSS-imide) at feed pressures of 2 bar up to a temperature of 300°C [9]. Simulations

at the higher temperatures of 100°C, 200°C and 300°C were thus also performed with loadings of CO_2 and CH_4 corresponding to a pressure of ~2 bar for both the 6FDA and PMDA poly(POSS-imide) models. Averages were made over the three independant samples in both cases. Initial estimates of the number of molecules to add were made using the infinite dilution solubilities and Eq. 4. In general, at these higher temperatures where the solubility is reduced, these initial estimates gave converged pressures sufficiently close to 2 bar not to warrant further iterations. Only in the case of CO_2 at 100°C were successive loadings required in order to obtain pressures close to the required value. In order to obtain estimates for the diffusion coefficients of penetrant gases, these simulations at 2 bar were extended out to a total of 30000 ps at 100°C and 10000 ps at 200 and 300°C.

To obtain the permeability coefficient P_i of a particular gas species *i*, the relation:

$$P_i = D_i \times S_{c_i} \tag{15}$$

is used where D_i is the corresponding gas diffusion coefficient in the matrix. To obtain the diffusion coefficients, the mean-squared displacements (MSDs) of the penetrant molecules were extracted from the simulations according to:

$$\left\langle \Delta R_i^2(t) \right\rangle = \frac{1}{n_{pol_i}} \left\langle \sum_{j=1}^{n_{pol_i}} \left(\vec{R}_j(t+t_0) - \vec{R}_j(t_0) \right)^2 \right\rangle \tag{16}$$

where $\vec{R}_j$ is the vector position of the centre-of-mass of penetrant molecule *j*. Averages are performed over all possible time origins t_0 and all n_{pol_i} penetrant molecules. Estimates of the diffusion coefficients can then be obtained from:

$$D_i = \lim_{t \to \infty} \frac{\left\langle \Delta R_i^2(t) \right\rangle}{6t} \tag{17}$$

3. Results and Discussion

3.1. Infinite dilution gas solubilities, mean insertion energies and *FSV*

This section presents the results of the EVMS TPI analyses on the pure poly(POSS-imide)s and uncrosslinked mixtures. The infinite dilution solubility coefficients determined using Eq. 7 are given in Table 1 for both poly(POSS-imide)s at 35°C, 100°C, 200°C and 300°C as well as for the corresponding 2:1 dianhydride+POSS uncrosslinked mixtures at 35°C. Also shown in Table 1 are the weighted mean test particle insertion energies, $\left\langle \Delta\Phi \right\rangle$, obtained from Eq. 12. The third quantity given in Table 1 is fraction of significant volume (*FSV*) that is responsible for 99.9% of the solubility (Eq. 14).

At 35°C, the reliability of the average solubilities given in Table 1 (as reflected by the associated standard error bars) is reasonably good for the four gases under study. The underlying Boltzmann-weighted distributions, $\rho_w(\Delta\Phi)$, given in a normalized form for the 6FDA poly(POSS-imide) in Fig. 2, confirm that convergence is good at 35°C for N_2, O_2, CH_4 and CO_2. Higher temperatures naturally lead to better convergence of the $\rho_w(\Delta\Phi)$ as the Boltzmann factor is reduced. Higher temperatures significantly reduce the average solubilities too for the same reason and the effect is compounded by the thermal dilation of the systems which reduce the interaction energies; this can be seen in the distributions in Fig. 2 and the mean insertion energies in Table 1 moving to less negative values as the temperature increases.

Table 1. The infinite dilution solubility coefficients (in cm^3(STP) cm^{-3} bar^{-1}) (**in bold**), the mean insertion energies (in kJ/mole of insertions) and the *%FSV* (*in italics*) for the different gases in the poly(POSS-imide)s and uncrosslinked mixtures.

Temperature	System	Property	N_2	O_2	CH_4	CO_2
35°C	PMDA poly(POSS-imide)	$S_c(0)$ $\langle\Delta\Phi\rangle$ *%FSV*	**2.72±0.02** -17.5±0.3 *1.50±0.05*	**3.63±0.03** -18.1±0.3 *1.82±0.06*	**9.0±0.3** -22.8±0.6 *1.08±0.04*	**177±4** -36.4±0.2 *0.67±0.04*
	6FDA poly(POSS-imide)	$S_c(0)$ $\langle\Delta\Phi\rangle$ *%FSV*	**2.81±0.11** -17.5±0.1 *1.28±0.05*	**3.63±0.11** -17.8±0.1 *1.60±0.06*	**9.1±0.5** -22.2±0.2 *0.90±0.04*	**190±10** -36.5±0.4 *0.57±0.02*
	2:1 PMDA+POSS mixture	$S_c(0)$ $\langle\Delta\Phi\rangle$ *%FSV*	**0.24±0.01** -20.1±1.0 *0.051*	**0.45±0.01** -20.1±0.7 *0.088*	**0.81±0.04** -25.8±2.0 *0.022*	**17.0±0.6** -38.2±1.9 *0.012*
	2:1 6FDA+POSS mixture	$S_c(0)$ $\langle\Delta\Phi\rangle$ *%FSV*	**0.300±0.004** -18.8±0.4 *0.088*	**0.56±0.01** -19.2±0.1 *0.144*	**0.80±0.02** -23.6±0.9 *0.041*	**21.7±0.4** -37.4±1.1 *0.023*
100°C	PMDA poly(POSS-imide)	$S_c(0)$ $\langle\Delta\Phi\rangle$ *%FSV*	**0.72±0.02** -16.0±0.2 *1.72±0.06*	**0.93±0.02** -16.4±0.2 *2.08±0.07*	**1.68±0.05** -20.7±0.4 *1.25±0.05*	**14.1±0.3** -32.6±0.1 *0.94±0.03*
	6FDA poly(POSS-imide)	$S_c(0)$ $\langle\Delta\Phi\rangle$ *%FSV*	**0.72±0.02** -16.2±0.1 *1.47±0.02*	**0.92±0.02** -16.3±0.1 *1.83±0.02*	**1.68±0.05** -20.6±0.2 *1.04±0.01*	**14.0±0.4** -32.2±0.1 *0.77±0.01*
200°C	PMDA poly(POSS-imide)	$S_c(0)$ $\langle\Delta\Phi\rangle$ *%FSV*	**0.21±0.01** -14.4±0.1 *2.06±0.04*	**0.27±0.01** -14.6±0.1 *2.49±0.05*	**0.36±0.01** -18.5±0.2 *1.50±0.02*	**1.46±0.05** -28.2±0.2 *1.21±0.03*
	6FDA poly(POSS-imide)	$S_c(0)$ $\langle\Delta\Phi\rangle$ *%FSV*	**0.207±0.002** -14.8±0.1 *1.76±0.04*	**0.265±0.002** -14.9±0.1 *2.18±0.05*	**0.36±0.01** -18.9±0.1 *1.22±0.03*	**1.49±0.01** -28.5±0.1 *0.97±0.03*
300°C	PMDA poly(POSS-imide)	$S_c(0)$ $\langle\Delta\Phi\rangle$ *%FSV*	**0.118±0.005** -12.9±0.1 *3.0±0.1*	**0.145±0.005** -13.1±0.1 *3.6±0.1*	**0.168±0.007** -16.6±0.1 *2.2±0.1*	**0.45±0.02** -24.7±0.2 *1.9±0.1*
	6FDA poly(POSS-imide)	$S_c(0)$ $\langle\Delta\Phi\rangle$ *%FSV*	**0.109±0.002** -13.4±0.1 *2.54±0.05*	**0.138±0.002** -13.5±0.1 *3.09±0.05*	**0.157±0.003** -17.1±0.1 *1.81±0.04*	**0.43±0.01** -25.3±0.1 *1.49±0.04*

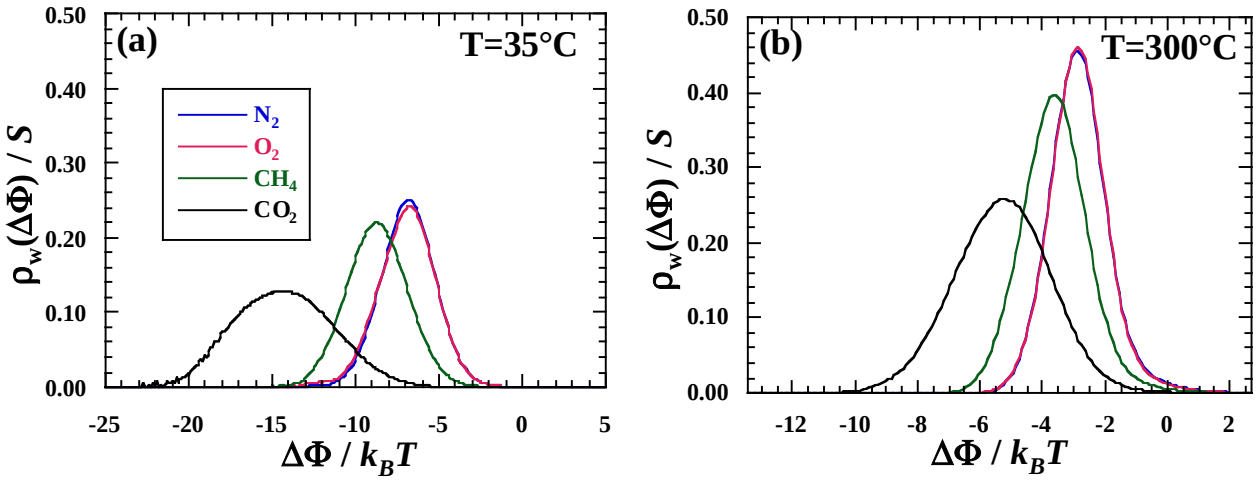

Figure 2. The normalized Boltzmann-weighted density distributions of test-particle insertion energies, $\frac{\rho_w(\Delta\phi)}{S}$, as obtained from the TPI analyses for the different gas probes in pure 6FDA poly(POSS-imide) systems at (a) 35°C and (b) 300°C. The x-axis of the right plot has been adjusted so that the range shown covers the same as that of the left plot when taking into account the different absolute temperatures.

In general the solubility coefficients and absolute values of the mean insertion energies for a given system at a given temperature follow the hierarchy $N_2 \approx O_2 < CH_4 < CO_2$, in agreement with the correlation seen in polymers between S_c and the critical temperature [66]. For the poly(POSS-imide)s, the 6FDA and PMDA forms give very similar results at the different temperatures studied, even though the volume fraction of the organic phase is higher in the former. This can be attributed to the shorter stiffer PMDA group leading to more steric hindrance and a higher proportion of available space than the longer flexible 6FDA group [11, 20]. This tendency for the available space to be slightly higher in the PMDA poly(POSS-imide)s can clearly be seen in the *%FSV* (Table 1). In general the *%FSVs* are in the order $O_2 > N_2 > CH_4 > CO_2$ at all the temperatures studied. The *%FSV* being based on energetic criterion, there tends to be more of a correlation with the solubilities than estimates of gas diameters [66]. As expected, increasing the temperature leads to higher *%FSV* but to differing extents. The *%FSV* of O_2, N_2 and CH_4 approximately double in going from 35°C to 300°C. For CO_2, there is roughly a factor of three between these two extremes. The *%FSV* underline the fact that different probes do not need to access the same amount of the available space in order to account for 99.9% of the solubility. Simple geometric measures of available volume can be misleading in this respect.

The results for all probes shows that the inherent higher number densities of the mixtures [19, 20] at 35°C lead to slightly more favourable insertion energies but considerably lower %*FSVs*. It is thus mostly this latter difference that accounts for the ~10 times higher infinite dilution solubility coefficients of the different probes in the poly(POSS-imide)s. This is one of the main consequences of cross-linking.

A comparison of the mixtures reveals that the probes have lower insertion energies and *%FSV* in the PMDA+POSS mixtures and, in most cases, a lower solubility. This indicates a closer packing in the PMDA case compared to 6FDA. It is known that the low polarity of fluorine gives a low refractive index, a low dielectric constant, while free volume is increased [67]. The -CF_3 groups do create slightly more space in the uncrosslinked 6FDA+POSS mixtures but this effect seems to be *in fine* less important than the steric hindrance imparted by the stiffer PMDA groups following imidization.

3.2. Sorption isotherms for carbon dioxide and methane at 35°C

The uptake curves at 35°C for CO_2 and CH_4 in the poly(POSS-imide)s and the related uncrosslinked mixtures have been determined as described in Section 2.7. In each of the comparative graphs presented hereafter, (a) will be for methane and (b) for carbon dioxide. For clarity, the legend, which will be the same for both graphs, will just be shown in (a). The results are first presented in Fig. 3 in terms of the actual *numbers of molecules* that are sorbed during the uptake phase. As all systems contain the same number of POSS moieties (216), the capacity of the 6FDA-containing systems to absorb more of the penetrants is clearer in this representation. The inorganic POSS cages being impermeable to the penetrant gases [18], the differences in uptake can be largely explained by the greater proportion of organic phase in the 6FDA-based systems. Indeed, probe accessible volume [23, 68] estimates of the volume fraction of organic phase in the pure systems are ~0.62 in the PMDA cases and ~0.70 in the 6FDA cases. To further emphasize this point, the actual average volumes of the simulation boxes of the different systems during sorption are plotted in Fig. 4. These are straightforward to extract as the ***NPT*** simulations allow the volume to adjust naturally. The plots show, for the same number of POSS moieties, the much higher volumes of the 6FDA systems which result from their higher organic phase content. It is important to bear in mind these inherent differences in the discussions that follow. More will be said later of the changes in volume seen during sorption.

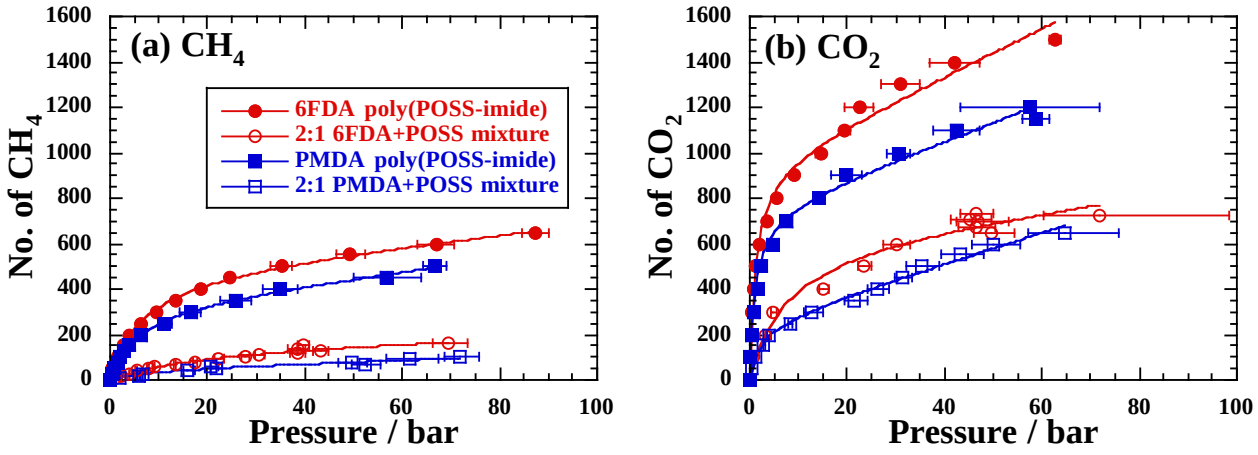

Figure 3. The number of (a) methane and (b) carbon dioxide molecules sorbed by the poly(POSS-imide)s and uncrosslinked mixtures as a function of the pressure. Errors in the estimation of the pressure of the gas reservoir in equilibrium with the fixed uptake are shown as horizontal bars and can be quite large at higher pressures for the reason explained in Section 2.7. The smooth lines are shown as a guide for the eye.

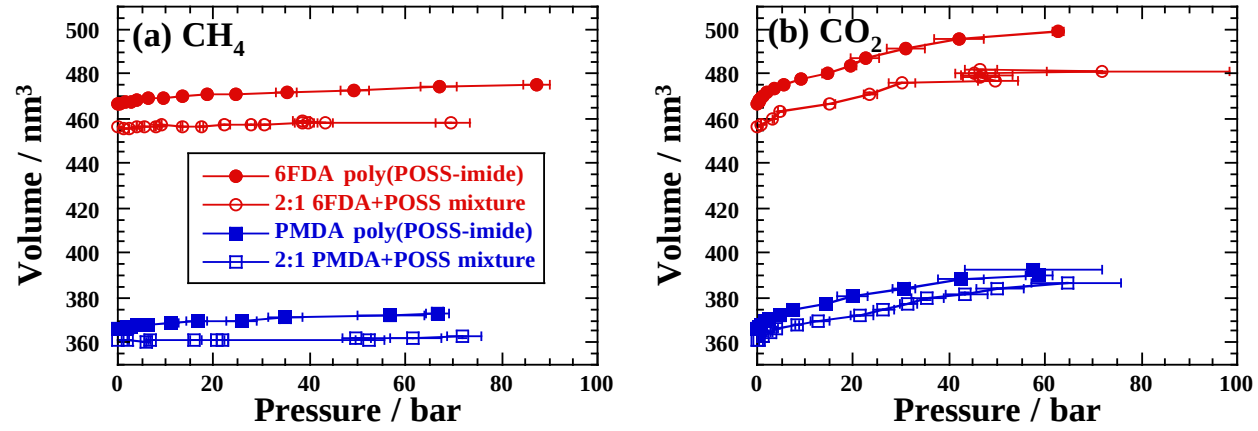

Figure 4. The average volumes of the simulation boxes of the poly(POSS-imide) and uncrosslinked mixture systems as a function of the pressure during (a) methane and (b) carbon dioxide sorption. The volume swelling due to sorption of the penetrants is clear to see.

In Fig. 5 we replot the uptake curves using the true concentrations (Eq. 5) of the penetrants in the different systems. In terms of concentrations, the results for the 6FDA and PMDA poly(POSS-imide)s show fairly similar behaviour as the greater inherent volumes of the 6FDA MD boxes (Fig. 4) compensate for the larger number of sorbed molecules (Fig. 3). As the volume of inorganic (inaccessible) phase is the same in both types of poly(POSS-imide), this again shows that the poorer packing induced by

the stiffer PMDA groups leads to a higher sorption capacity than what could be expected. It also confirms that the poly(POSS-imide)s have significantly higher solubilities than the uncrosslinked mixtures resulting from the steric hindrance imparted by the cross-links.

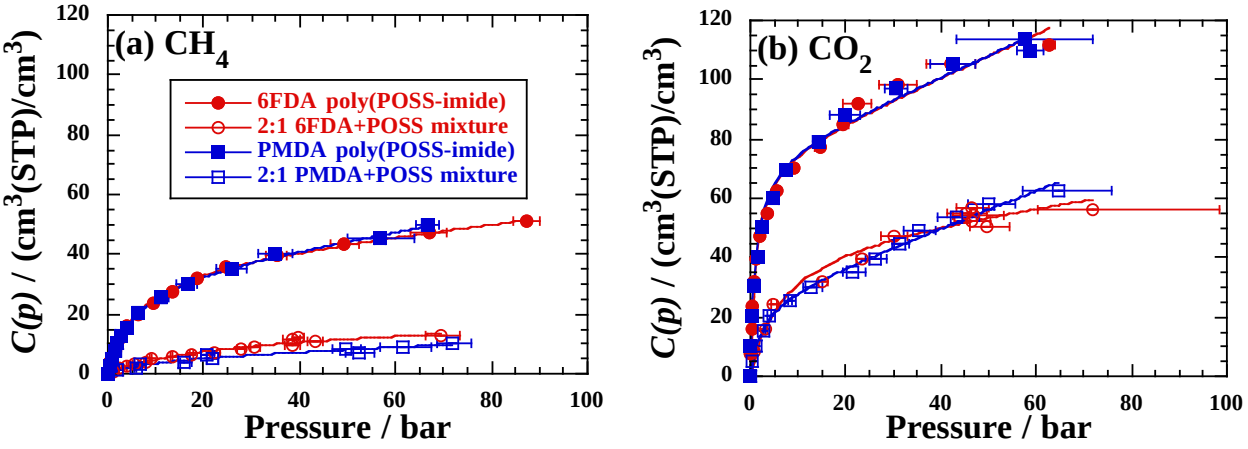

Figure 5. The concentrations of (a) methane and (b) carbon dioxide molecules sorbed by the poly(POSS-imide)s and uncrosslinked mixtures as a function of the pressure. Errors in the concentrations are shown but are generally less than the size of the symbols. The smooth curves are fits to the DMS model [62] (Eq. 8).

The smooth curves shown in Fig. 5 are non-linear least squares regression fits to the dual-mode sorption (DMS) model [62] given in Eq. 8. There is no intention here to justify the DMS model, for which there are a certain number of criticisms [69, 70]. We simply use the functional form of Eq. 8 as a common and familiar way of fitting smooth curves to the sorption curves.

The actual solubility coefficients (Eq. 6) are plotted in Fig. 6 as a function of the penetrant concentration. In the poly(POSS-imide)s, the solubility coefficients fall rapidly as the concentration increases. For both CH_4 and CO_2, the values at ~50 $cm^3(STP)cm^{-3}$ have already been reduced by a factor of ten, i.e. roughly equivalent to those of the respective mixtures at infinite dilution. Surprisingly, there is little evidence of an initial linear dependence on concentration in these systems, as would be expected from a Langmuir mechanism.

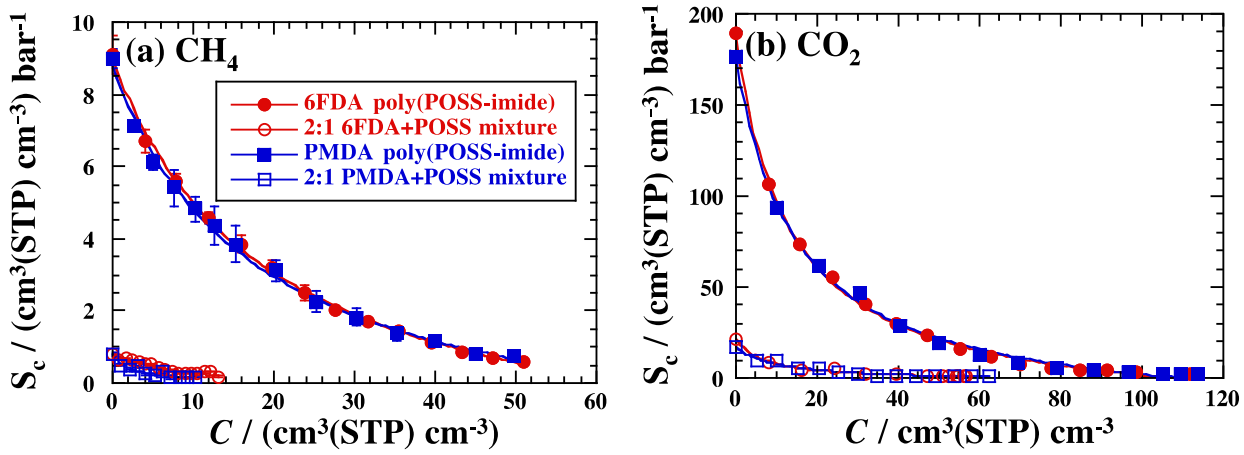

Figure 6. The solubility coefficients of (a) methane and (b) carbon dioxide molecules sorbed by the poly(POSS-imide)s and uncrosslinked mixtures plotted as a function of the concentration of the respective penetrants. The smooth curves are fits to the DMS model [62] (Eq. 8).

As the concentrations increase, the solubility coefficients tend towards a plateau value concomitant with a Henry's law sorption and there are at least three reasons for this:- (a) volume swelling can occur, (b) chain packing can change in order to accommodate more penetrant molecules and (c) the gradual increase in penetrant concentration can have an effect on the interaction energy $\Delta\Phi$ of further penetrants. The relative volume change, $\varepsilon_V = \left(V - V_0\right)/V_0 = \Delta V / V_0$ where V is the volume of the loaded system and V_0 is the volume of the pure system, are shown in Fig. 7.

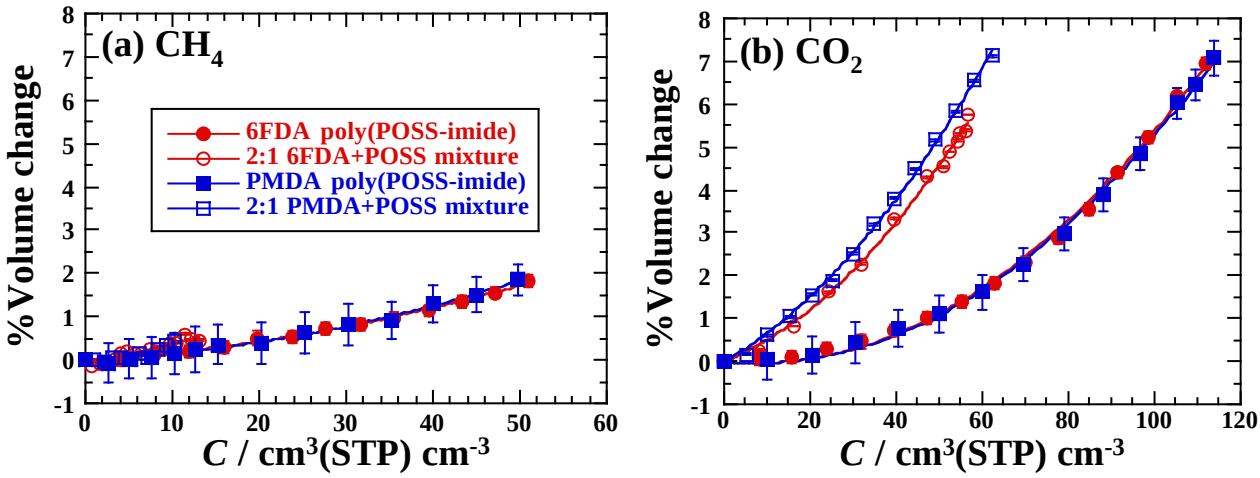

Figure 7. The volume change occuring during sorption of (a) methane and (b) carbon dioxide molecules in the poly(POSS-imide)s and uncrosslinked mixtures plotted as a function of the concentration of the respective penetrants.

It can be seen from Fig. 7 that the swelling is progressive and the rate tends to increase with penetrant concentration. Although it can be expected that dilation tends to a linear asymptote, the data has been fitted to a simple function of the form $\varepsilon_V = a_1 C + a_2 C^2$ over the interval shown; these are the smooth lines shown in Fig. 7. The swelling appears to be greater in the mixtures compared to the poly(POSS-imide)s since the absence of cross-linking leads to better packing and thus a lack of space for the penetrants. This is more evident in the case of CO_2 where the concentrations attained are much higher. There is also slightly less swelling in the 6FDA mixture which is consistent with its greater initial *%FSV*, as already discussed. In the poly(POSS-imide)s, the dilation is similar for 6FDA and PMDA systems despite the fact that, as noted above, the PMDA has a lower organic (penetrant accessible) volume fraction (0.62 as compared to 0.70 for 6FDA). As the total concentration vs. pressure curves are very similar (Fig. 5), this implies that there is a higher penetrant concentration in the organic phase of the PMDA system compensating for its lower organic volume fraction. To illustrate this, the swelling of the organic phase has been estimated. This is possible as probe accessible volume tests [23, 68] show that the inorganic (penetrant inaccessible) phase volume is constant irrespective of the loading. The results for CO_2 are plotted as a function of the corresponding organic phase concentration in Fig. 8. The smooth lines are fits to the same form as for Fig. 7. When compared to the results of the total swelling (Fig. 7b), the lower swelling of the organic phase in the PMDA poly(POSS-imide) is clear to see in Fig. 8, whereas for the mixtures there are hardly any changes. The higher *%FSV* of the PMDA poly(POSS-imide) thus leads to the delayed swelling and higher sorption capacity of its organic phase.

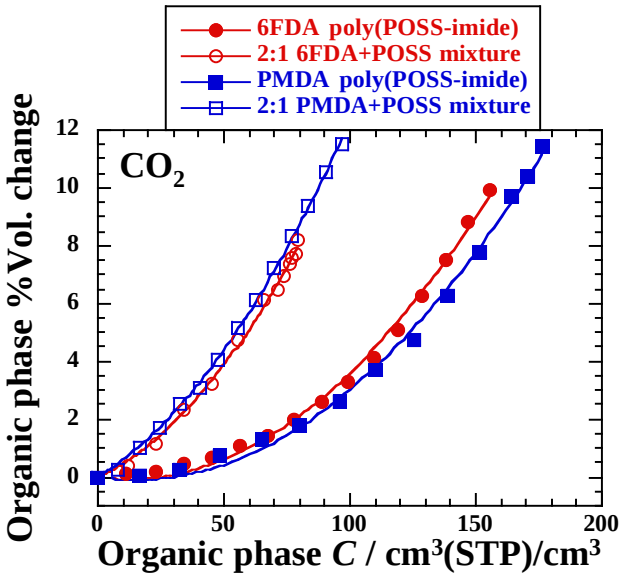

Figure 8. The estimated volume change occuring in the organic phase during sorption of carbon dioxide molecules in the poly(POSS-imide)s and uncrosslinked mixtures plotted as a function of the concentration of CO_2 in the organic phase in cm^3 (STP) of gas per cm^3 of organic phase. Error bars are omitted for clarity.

Although, ultimately, the swelling is considerably higher for CO_2 than that observed for methane, because of its higher solubility and the accelerating rate of swelling at higher concentrations, the average swelling provoked *per molecule* is greater in the case of methane at equivalent concentrations. This can be seen in Figure 9, where the volume change divided by the number of penetrants is plotted as a function of the penetrant concentration in the organic phase. In the range of concentrations that can be compared, the average methane swelling per molecule is ~5 $Å^3$ (~3 cm^3/mole) higher than that of carbon dioxide. This is consistent with the difference in partial molar volumes of the two molecules in their respective low-temperature crystalline (closest-packed) phases [71, 72]. The differences between the 6FDA and PMDA systems for CO_2 in Fig. 9 occur for the same reasons as those discussed for Fig. 8.

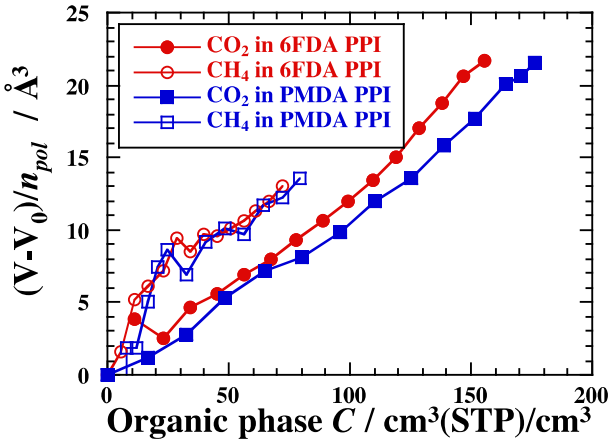

Figure 9. The average volume swelling induced per molecule of penetrant as a function of the concentration of penetrants in the organic phase of the different poly(POSS-imide)s. Error bars are omitted for clarity. In the legends, PPI refers to poly(POSS-imide).

The corresponding changes in the fractions of significant volume *FSV* (Eq. 14) are presented as percentages in Fig. 10. The initial rapid reduction of the *%FSV* to relatively low values, as the penetrants fill the available holes, leads to the acceleration in the volume swelling that occurs in the poly(POSS-imide)s in the organic phase concentration range from ~75-100 $cm^3(STP)/cm^3$ (Fig. 8). The greater accessible volume of the PMDA poly(POSS-imide)s is clear to see up to concentrations of ~100 $cm^3(STP)/cm^3$ and, although it is not possible to see on the scale of Fig. 10, the difference persists over the entire range studied. The rather marked initial differences in the *%FSV* of both penetrants diminish as the concentration increases due to those for methane decreasing at a more rapid rate before ~50 $cm^3(STP)/cm^3$. This correlates with the results shown in Fig. 9 which imply that CH_4 occupies a larger volume than CO_2. As already discussed, the initial lower *%FSV*s of carbon dioxide are consistent with the trends seen in Table 1 where the probes which interact more with the matrices have the lower *%FSV*s.

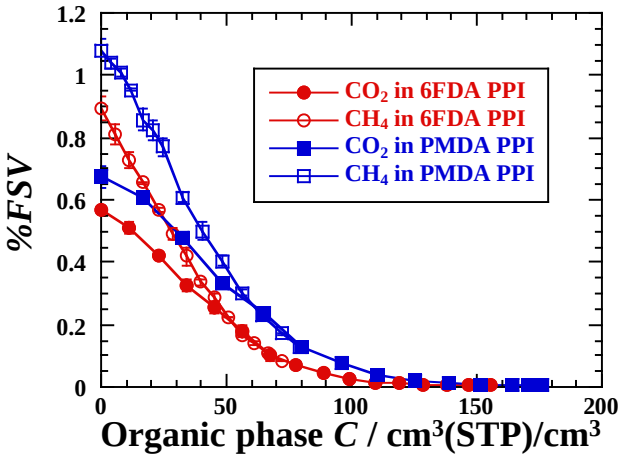

Figure 10. The behaviour of the fractions of significant volume required to obtain 99.9% of the solubility (Eq. 14), expressed as percentages, as a function of the concentration of penetrants in the organic phase for the different poly(POSS-imide)s during the sorption simulations.

The effect of sorption can also be seen in the changes to the underlying Boltzmann-weighted distributions of insertion energies, $\rho_w(\Delta\Phi)$, at successive loadings. An example is given in Fig. 11a for carbon dioxide uptake in the 6FDA-poly(POSS-imide). At the start of volume dilation, there is an initial marked effect on the $\rho_w(\Delta\Phi)$ with a notable decrease in solubility and an abrupt shift in the peak position toward less negative energies. As the loading increases, there is a tendency for the distributions to shift back towards lower energies. This trend can be seen also in the behaviour of the average insertion energies (Eq. 12) which are plotted in Fig. 12 for both poly(POSS-imide)s and penetrants.

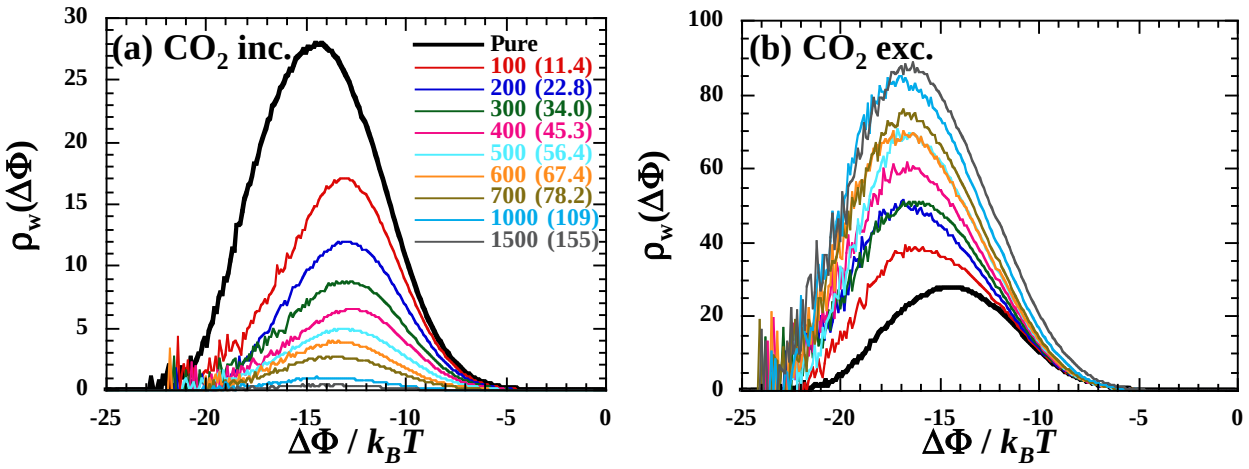

Figure 11. The Boltzmann-weighted distributions of insertion energies, $\rho_w\left(\Delta\Phi\right)$, for (a) CO_2 probe test particle insertions at a selection of different CO_2 loadings in the 6FDA-poly(POSS-imide) system at 35°C. The numbers in the legend correspond to the numbers of sorbed CO_2 molecules and the figures in brackets are the approximate corresponding concentrations in cm^3(STP)/cm^3 of organic phase. Figure (b) is as (a) except that the TPI probe molecule does not interact with the sorbed CO_2 already present in the systems.

It is tempting to attribute the initial shift in the $\rho_w\left(\Delta\Phi\right)$ towards less negative energies to a preferential filling of the lowest energy sites in the matrix, similar to the mechanism proposed by Kirchheim [70]. In reality, a closer inspection reveals a more complex behaviour. By analysing the loaded systems using TPI in which the probe molecule *does not interact* with the sorbed penetrant molecules, information can be obtained as to the effects sorption has on the matrix itself. Such (penetrant-excluded) distributions were systematically determined for all systems and loadings and, as an example, Fig. 11b shows the distributions corresponding to Fig. 11a; qualitatively, the results for CO_2 in the PMDA poly(POSS-imide) and CH_4 in both poly(POSS-imide)s were similar. The distributions in which the sorbed penetrants do not interact with the probe are displaced to lower energies and are of a higher peak height. As such, the matrix can not be considered as being a static environment into which the penetrants are loaded. Even at the lowest loadings, where volume swelling is insignificant (Figs. 7 and 8), the interactions of sorbed CO_2 molecules with the matrix adjust the latter in a way that leads to the *apparent* increase in the quantity of favourable lower energy sorption sites seen in Fig. 11b; of course, actual removal of the sorbed CO_2 would permit the matrix to relax and the distribution would again approach that of the pure system. Comparisons (not shown) of the radial distribution functions, as evaluated during the EVMS-TPI analyses, for the CO_2 probe with the different types of atoms in the matrices of the pure

poly(POSS-imide)s with those for the systems loaded with 100 CO_2 (in which the penetrants are not seen by the probe) reveal that these adjustments take place particularly around the -NH_2 groups at the ends of the unlinked POSS arms, i.e. those having the most liberty of movement.

This shift of the distributions shown in Fig. 11b to lower energies also correlates with the behaviour of the CO_2-excluded *%FSV* (not shown) which tend to decrease slightly before increasing again as the volume starts to swell. Tests also reveal that the majority of these adjustments occur within the first 10 ps following insertion of the penetrants which would confirm relatively subtle underlying changes to the matrix. Similar changes have been seen in the case of CO_2 conditioning of explicit models of polyimide membranes [60].

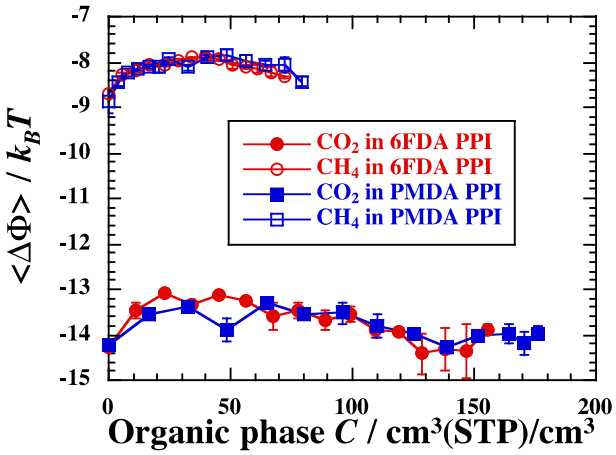

Figure 12. The mean insertion energies for CO_2 and CH_4 probe test particle insertions in the poly(POSS-imide)s at 35°C as a function of the penetrant concentrations in $cm^3(STP)/cm^3$ of organic phase.

3.3. Desorption isotherms for carbon dioxide in poly(POSS-imide)s at 35°C

As seen in the previous sections, exposure to CO_2 at high pressures leads to significant volume swelling (Figs. 7 and 8). On experimental time scales, subsequent hysteresis is often seen in the desorption curves [13, 22]. For this reason, the poly(POSS-imide) systems containing CO_2 also had their desorption curves determined. The method, explained in Section 2.7, first involved extending the simulations at the highest loadings shown in Fig. 3 out to 20000 ps in order to assess, albeit to a relatively limited extent, the effects that relaxation under high loading can have compared to those seen experimentally [52-59]; a discussion of these relaxation effects is reserved for the next section, in which we describe additional longer simulations that have been performed at even higher loadings. The resulting concentrations of CO_2 during desorption are shown in Fig. 13a along with the corresponding sorption curves. Hysteresis is visible despite the limited time of exposure and is similar for both types of

poly(POSS-imide). The main reason can be seen in Fig. 13b where the slow relaxation of the matrices following the removal of CO_2 also leads to hysteresis in the volume swelling. This is similar to the behaviour seen before in model glassy 6FDA-based polyimide systems [44, 60] although the limiting residual swelling (<1%) is smaller in the case of these poly(POSS-imide)s. In addition, during the 10000 ps following the complete removal of all the penetrants, it continues to diminish to ~0.3% for both poly(POSS-imide)s. This almost complete recovery is in agreement with experimental findings where it has been attributed to the stability afforded by the high degree of crosslinking [13].

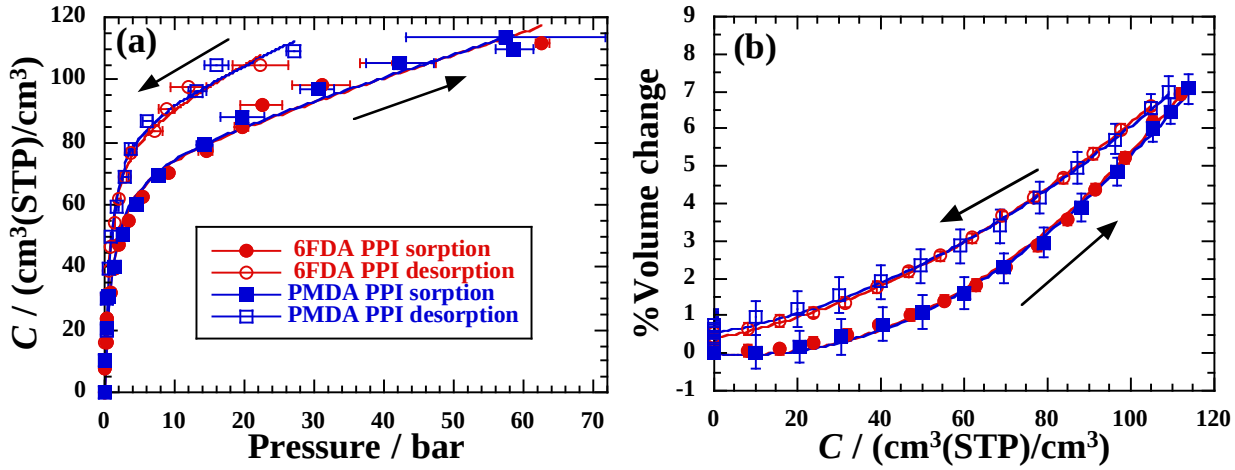

Figure 13. (a) the concentrations of CO_2 molecules in the poly(POSS-imide)s as a function of the pressure during sorption (filled symbols) and desorption (open symbols). The smooth curves are fits to the DMS model [62] (Eq. 8). (b) the corresponding plot for the % volume changes. Smooth curves are fits to quadratic functions.

To investigate further how the volume hysteresis influences the solubility, the *%FSV*s and mean insertion energies during the desorption were examined. Plots (not shown) of the results reveal that there is no detectable hysteresis in the *%FSV*s whereas the $\langle \Delta\Phi \rangle$ are clearly more negative during desorption. Comparisons of the underlying $\rho_w(\Delta\Phi)$ (also not shown) show that this results from a shift of the peaks to more negative energies during desorption caused by an increase in amount of the low and intermediate energy sites. The distributions at the higher energy side are largely unchanged which explains the relative invariance of the *%FSV*s.

3.4. Comparisons with experiments for 6FDA poly(POSS-imide)s at 35°C

As stated in the introduction, experimental studies of CO_2 and CH_4 sorption and swelling in supported thin films of 6FDA poly(POSS-imide)s have been carried out at 35°C and up to pressures of 60

bar [13]. This particular study demonstrated the extreme sensitivity of the sorption curves to the initial concentration of the aqueous POSS solution used in the interfacial polymerization reaction step. Concentrations of 0.9, 2.5 and 5 wt % of POSS were used and, in the resulting films, these led to large variations in the uptakes of CO_2 and CH_4 and in the associated volume dilations [13]. The study also revealed the higher sorption capacities of the organic-inorganic network films compared to two types of polyimides and several other polymers [61]. XPS analyses of the crosslinked films indicated that higher POSS concentrations in the initial solutions led to lower ratios of POSS to imide groups, i.e. lower numbers of links between POSS cages. Although precise values of these ratios are difficult to obtain from XPS measurements, the range was estimated to vary from ~4.9 for the 0.9 wt % case to about ~3.7 for the 5 wt % case. Indeed our chosen simulated value of 4 was based on these estimations.

Comparisons with the experimental results for the sorption of CO_2 in the 6FDA poly(POSS-imide) indicate that the simulated results do correspond closest to those obtained for the 5 wt % experimental film. The experimental results for this particular film are plotted in Figure 14 along with those obtained in the present simulations.

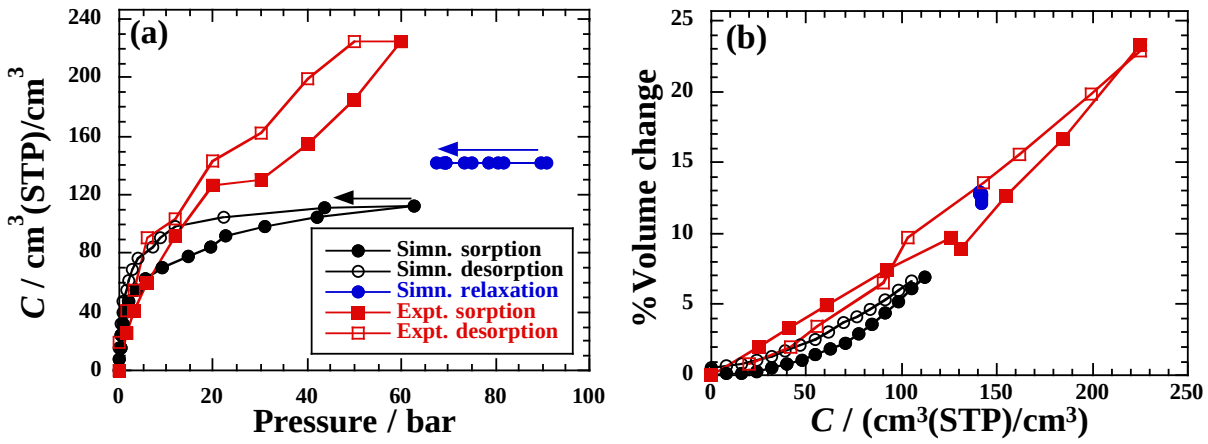

Figure 14. A comparison of the results obtained from the simulations for the uptake of CO_2 in the 6FDA poly(POSS-imide) with the experimental results of Raaijmakers *et al*. [13] for their 5 wt % film. In (a), the concentration vs. pressure curves are shown for both the sorption and desorption. The relaxation of the pressure (see text for details) over 20000 ps and 41000 ps for the simulated systems at loadings of 1500 and 2000 CO_2 are indicated by the black and blue arrows, resp. In (b), the corresponding volume changes are shown as a function of the CO_2 concentration. For clarity error bars are omitted.

In Fig. 14a, the concentrations are plotted as a function of pressure and although both the experimental and simulated curves show similar hysteresis loops, the simulated sorption tends to overestimate the

uptake at lower pressures and underestimate it at higher pressures. Overestimates at low pressures are not uncommon in simulations [73-75] and have been attributed [44] primarily to the limited amount of long-time relaxations and physical ageing [76] on the restricted time scale accessible to MD and the total absence of residual solvents and other contaminants rather than to inadequacies in the force field; in the specific case under study here, we cannot rule out the influence of the simplifications in the models (e.g. all T8 cages being intact, see Section 2) nor the sensitivity to the connectivity. Underestimates are less common but, in the case of highly soluble penetrants such as CO_2, the exposure (or conditioning) time has also to be considered. It is well-known that relaxation times in 6FDA-based polymers can be extremely long [56, 57]. Indeed, tests of the effect of an incremental CO_2 pressure rise from zero to 50 bar in a 6FDA poly(POSS-imide)s have shown that, although there is a rapid uptake of CO_2, there can also be an important secondary relaxation which is clearly evident over a period of at least 40 hours [13].

To investigate further the effect of prolonged exposure and relaxation at high concentrations, some additional simulations were performed on all three samples of the 6FDA poly(POSS-imide). Starting from the configurations containing 1500 CO_2, i.e. the highest loadings shown in Fig. 3b, loading was continued in steps of 100 CO_2 up to the insertion of 2000 CO_2 using the same protocol as described in Section 2.7. The systems were first simulated for a period of 3000 ps at the required pressure of 60 bar. The last 2000 ps were analysed by TPI and the iterative technique was then applied. If no solution to the equality of chemical potentials for the CO_2 in the two phases (Eq. 4) was found up to pressures of 100 bar, the pressure was set to 100 bar for the next iteration. If a solution was found, then this pressure was applied for the next iteration. In both cases an iteration consisted of 2000 ps of ***NPT*** MD. During the first 15000 ps of the iterative procedure at this high loading no solution to Eq. 4 was found. The procedure was continued up to a total simulation time of 41000 ps, i.e 20 iterations. The behaviour of certain properties during the relaxation are shown in Fig. 15.

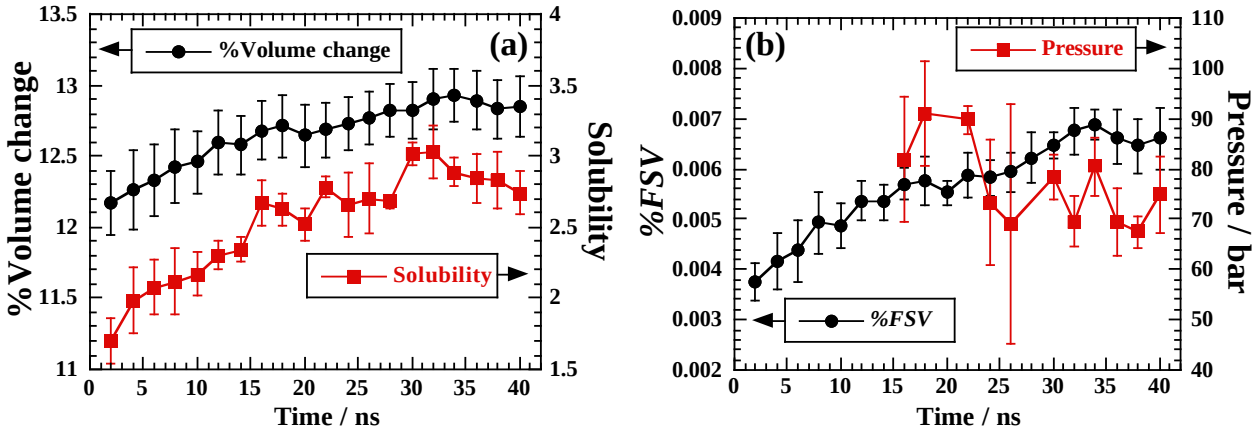

Figure 15. Plot (a) shows the relaxation of the average percentage volume change (left-hand scale) and the solubility (Eq. 3) of CO_2 (right-hand scale) as a function of time for the additional simulations carried out for 2000 CO_2 inserted in the 6FDA poly(POSS-imide) systems. Plot (b) shows the corresponding fractions of significant volume, Eq. 14, (left-hand scale) and the average pressure of the gas phase in equilibrium with the actual uptake (right-hand scale). Only after 15 ns of relaxation could an equality of chemical potentials for the CO_2 in the two phases (Eq. 4) be found.

It is clear from Fig. 15a that there is a gradual dilation of the volume of ~0.5% with time. Over the same period an approximate doubling of the solubility (Fig. 15a) and *%FSV* (Fig. 15b) occur and these are closely correlated to the volume dilation. Note that the solubility (Eq. 3) is shown in Fig. 15a rather than the solubility coefficient as the pressure corresponding to the equality of chemical potentials for the CO_2 in the two phases is not known when there is no solution to Eq. 4. Indeed, only after 15000 ps of relaxation has the solubility of the CO_2 in the 6FDA poly(POSS-imide) increased sufficiently for a solution to be found; the existence of a solution depends largely on this as the variation in the CO_2 concentration due to the volume dilation of ~0.5% seen in Fig. 15a is relatively small. The resulting (average) pressure is also plotted in Fig 15b whenever a solution is found in at least one of the three systems and its general trend is to diminish with time.

This relaxation of the pressure with time for the systems loaded with 2000 CO_2 is also shown in Fig. 14a (blue circles) along with those for the 1500 CO_2 containing systems. Both these results at high loadings suggest that the time of exposure is definitely a variable that has to be taken into account when attempting to simulate the sorption isotherms of these systems. The limited MD time scales restrict the exposure times that can be practically studied but the evidence is consistent with the shorter relaxation time being one of the reasons for an underestimation of the uptake at high loadings.

The corresponding comparison between the average simulated and the 5 wt % experimental film for the volume swelling during CO_2 sorption and desorption is shown in Fig. 14b. The initial delay in swelling seen in the simulated system is, like the solubility, consistent with a greater proportion of available volume arising from the relatively short period of physical ageing. At higher loadings in the range from $100 < [CO_2] < 200$ cm^3(STP) cm^{-3}, the experimental and simulated slopes are very similar and correspond to a partial molar volume for CO_2 of ~25 cm^3 mol^{-1}. As already mentioned, complete unloading leads to an almost full recovery of the volumes in both cases in these highly crosslinked materials.

For CH_4 sorption in the 6FDA poly(POSS-imide), the experimental results for the specific 5 wt % experimental film exceptionally give very similar results to those obtained for CO_2 sorption [13]; at ~60 bar the uptake is slightly in excess of 200 cm^3(STP) cm^{-3} and the corresponding volume swelling attains ~20%. However, uptakes of CH_4 at pressures of ~60 bar in the 2.5 wt % and 0.9 wt % experimental films are smaller than those for CO_2. These are more typical of the lower solubility methane generally has in glassy polymer membranes where the ratios of CH_4 to CO_2 concentrations at high pressures typically vary from ~0.2 to ~0.6 [59, 77-81]. The simulated results obtained here for CH_4 sorption in 6FDA poly(POSS-imide) give a ratio of ~0.4 which falls within this latter range.

3.5. Permeation of CO_2 and CH_4 in poly(POSS-imide)s at 100°C, 200°C and 300°C

As described in Section 2.8, additional simulations for the three independent samples of each type of poly(POSS-imide) have been performed at the higher temperatures of 100°C, 200°C and 300°C with loadings of CO_2 and CH_4 corresponding to a pressure of ~2 bar. Indeed, this pressure and temperature regime were used for experimental measurements of the permeation of several gases through supported films of 6FDA poly(POSS-imide) [9]. The actual numbers of molecules loaded into the systems are given in Table 2 as well as their average concentrations over the entire MD simulations. At a fixed applied pressure of 2 bar, the numbers of molecules inserted decreases with the temperature due to the lower solubility (Table 1). The mean solubility coefficients and estimated pressure were obtained as before.

Table 2. The number of gas molecules loaded into the samples that correspond to an applied pressure of 2 bar for both types of poly(POSS-imide) systems at the three different temperatures shown. The average concentrations of penetrants during the MD simulations are also shown.

		CH_4		CO_2	
Temp.	Poly(POSS-imide)	No. loaded	Concn. / cm^3(STP) cm^{-3}	No. loaded	Concn. / cm^3(STP) cm^{-3}
100°C	PMDA	34	3.448±0.005	160	16.12±0.04
	6FDA	43	3.415±0.001	200	15.81±0.05
200°C	PMDA	8	0.794±0.002	30	2.97±0.01
	6FDA	10	0.780±0.001	38	2.952±0.001
300°C	PMDA	4	0.384±0.001	10	0.959±0.002
	6FDA	4	0.303±0.001	10	0.755±0.001

In the case of penetrant diffusion in glassy polymer matrices, the rattle-and-hop mechanism [82-84] is generally observed whereby penetrants often spend long periods rattling around in cavities before making occasional hops to other sites when a channel between them opens up. The time scale required to obtain convergence of the diffusion coefficients can thus be longer than that which can be simulated directly [82, 85, 86]. The values obtained in this case from Eq. 17 are then best considered as upper bounds as $\left\langle \Delta R_i^2(t) \right\rangle / 6t$ is a monotonically decreasing function up until the Einstein regime, i.e. $\left\langle \Delta R_i^2(t) \right\rangle \propto t$, is attained. In certain circumstances, it is possible to obtain better estimates to limiting values of diffusion coefficients via the trajectory extending kinetic Monte Carlo (TEKMC) method [23, 86, 87]. The method depends critically on the identification of a percolating network of diffusion paths between the different sorption sites in the system within the time scale of the explicit MD simulation; an illustration of such a percolating network is shown in Figure 16. If this condition is fulfilled, an average probability matrix of jumps between sites can be determined from the MD-generated trajectories of the penetrants. This can then be used in a subsequent kinetic MC simulation which is able to extend the trajectories by a factor of 1000 at negligible computing cost. This was found to be the case here for CO_2, whereas for CH_4, a combination of a lower solubility and insufficient diffusion did not allow for the identification of a percolating network.

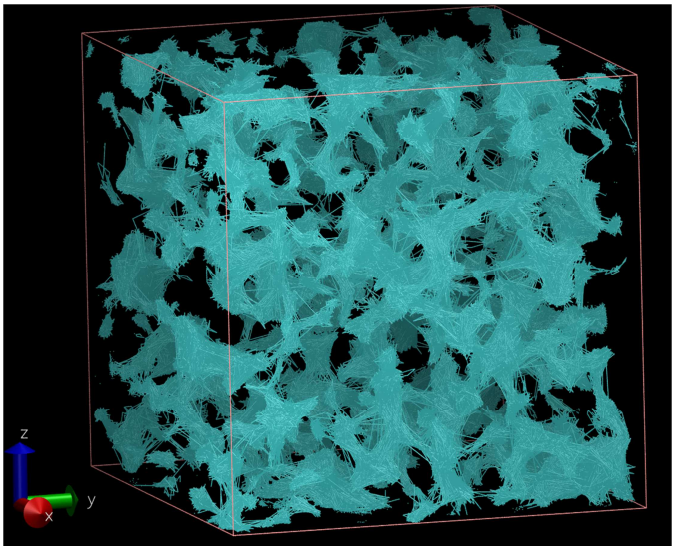

Figure 16. An illustration of the in-box trajectories of the central carbon atom of the 200 CO_2 molecules in one of the samples of 6FDA-poly(POSS-imide) at 100°C and a pressure of ~2 bar. A straight line is drawn between positions at an interval of 5 ps apart for a total simulation time of 30000 ps. Evidence of the rattle-and-hop mechanism [82-84] is clear to see as CO_2 molecules spend long periods localised in specific regions of space before making jumps through narrow transient channels to other sites. The image was rendered using VMD [88].

The results for the (upper bound) diffusion coefficients, obtained directly from the MD-generated trajectories using Eq. 17, are displayed as a function of the reciprocal temperature in Fig. 17a. These estimates of D show an Arrhenius-type behaviour with their natural logarithms being proportional to $1/T$. A slight deviation can be can be seen for CH_4 in the 6FDA poly(POSS-imide) at 300°C but the highest temperatures correspond to the lowest loadings and there is thus less precision in the results. This latter result apart, diffusion is in general slightly greater in the PMDA poly(POSS-imide)s, which is again consistent with its larger amount of available space. Also shown in Fig. 17a are the more reliable TEKMC estimates for the diffusion coefficient of CO_2. These are significantly lower, particularly at the lower temperatures, than those obtained directly from MD since the TEKMC-generated trajectories allow for the Einstein (plateau) regime to be attained. Nevertheless, they preserve the finding that the diffusion is slightly greater in the PMDA poly(POSS-imide)s.

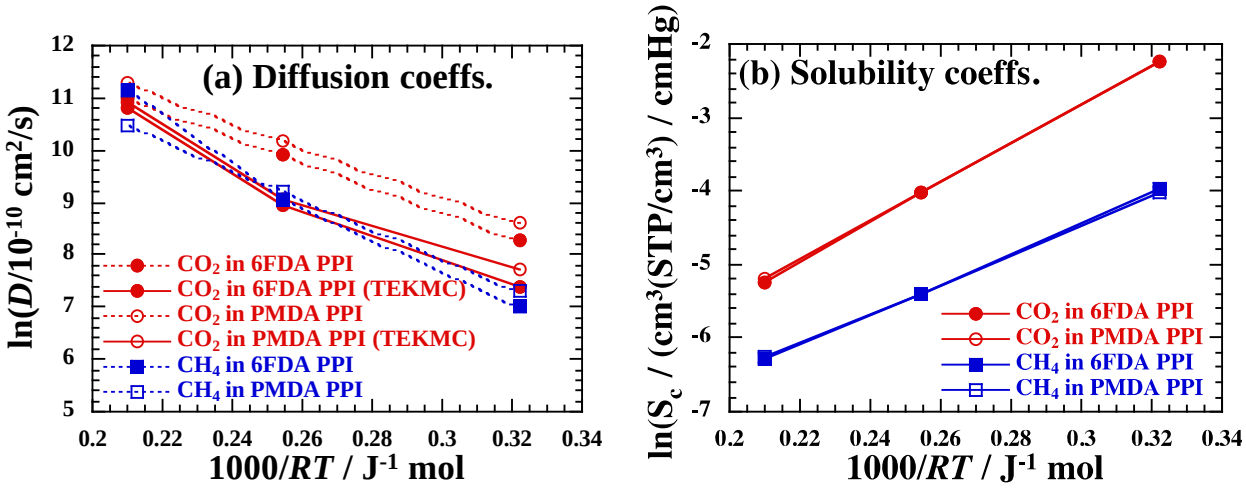

Figure 17. The natural logarithms of (a) the diffusion and (b) the solubility coefficients obtained from the simulations for CO_2 and CH_4 in the poly(POSS)-imides as a function of the inverse temperature. In (a), the more reliable TEKMC estimates of the diffusion coefficients are shown with solid lines.

As already found for the infinite dilution solubility coefficients (Table 1), the solubility coefficients at 2 bar are also very close and are practically indistinguishable on a logarithmic scale for the 6FDA and PMDA poly(POSS-imide)s in Fig. 17b; to be consistent with the barrer unit of permeability, the solubility coefficients are given here in $(cm^3(STP)/cm^3)/cmHg$. The solubility coefficients obey well the Arrhenius-type behaviour and the slopes of the plots give activation energies of ~26 kJ mol^{-1} for CO_2 and ~20 kJ mol^{-1} for CH_4, indicating that proportionally S_c for CO_2 decreases faster as temperature is increased.

The resulting permeability coefficients (Eq. 15), evaluated both from the MD and TEKMC (CO_2 only) estimates of D, are shown in Fig.18a. Upon heating, the permeabilities for CO_2 tend to remain rather independent of T, as the increase in D is compensated for by a fall in S_c. On the other hand, those for CH_4 tend to increase as the solubility coefficient is less affected by the increasing temperature. A similar qualitative behaviour has been seen in permeation experiments on 6FDA poly(POSS-imide) [9], albeit for thin films prepared in a different way and with a different cross-linking density than those compared to previously at 35°C [13]. The ideal gas separation factors, $\alpha = P_{CO_2} / P_{CH_4}$, are predicted from the simulations to remain relatively high at ~20 at 100°C to ~10 at 200°C for both 6FDA and PMDA poly(POSS-imide)s. Qualitatively, this trend is also in agreement with experiments [9].

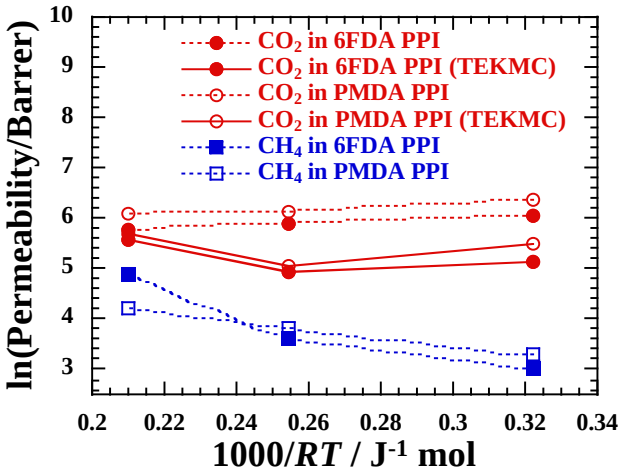

Figure 18. The natural logarithms of the permeability coefficients as a function of the inverse temperature for CO_2 and CH_4 from simulations in the two different poly(POSS)-imides. Dashed lines indicate permeabilities obtained from the solubility coefficients and the upper bound values of *D* using Eq. 15. For CO_2, values obtained using estimates of *D* from the TEKMC method are also shown (thick lines). Barrer is the unit of permeability coefficient that results from multiplying together a *D* in 10^{-10} cm^2/s and an S_c in $(cm^3(STP)/cm^3)$ /cmHg.

4. Conclusions

The sorption and permeation properties of two different poly(POSS-imide) crosslinked model networks have been successfully investigated. The dependence of the properties on the nature of two specific imide linkers has been determined and the effect of crosslinking has been characterized by comparing them to the (hypothetical) uncrosslinked mixtures of the same 2:1 dianhydride to POSS stoechiometry. The infinite dilution solubilities of the 6FDA and PMDA poly(POSS-imide)s are very similar as the lower organic (accessible) volume fraction of the PMDA form is compensated for by a larger proportion of available space due to the greater steric hindrance of the shorter stiffer PMDA linker. The *%FSV* reveal in particular that the uncrosslinked mixtures have infinite dilution solubilities ~10 times lower than the crosslinked poly(POSS-imide)s because of their much lower available spaces.

The single-gas sorption isotherms at 35°C for CO_2 and CH_4 in the poly(POSS-imide)s and uncrosslinked mixtures were obtained up to pressures of at least 60 bar. As for the infinite dilution solubilities, the concentration vs. pressure plots for the poly(POSS-imide)s are very similar for both penetrants. Volume dilation accelerates with loading as the *%FSV* rapidly diminishes. Due to its steric hindrance, swelling in the organic phase of the PMDA poly(POSS-imide) is lower than that in the 6FDA poly(POSS-imide). At equivalent concentrations in the organic phases the average swellings per penetrant

are found to be higher for CH_4 than CO_2 in the poly(POSS-imide)s. The Boltzmann-weighted distributions of insertion energies reveal subtle changes in the matrices.

The desorption isotherms at 35°C for CO_2 in the poly(POSS-imide)s show characteristic hysteresis. Comparisons were made with published experimental curves for 6FDA poly(POSS-imide)s [13]. At low pressures, the sorption in the simulations tends to overestimate that found experimentally. At high pressures, the simulated results underestimate the CO_2 uptake. The prolonged exposure at the highest concentration attained during sorption and further tests at even higher concentrations reveal the slow relaxations that can occur in the structures with time. Such a drift with time has the effect of bringing the simulated curve more into line with that of the experiment. The long-time relaxations of the networks and the duration of exposure are thus factors that cannot be ignored in the simulations.

Permeation measurements at higher temperatures show that the solubility coefficients behave in an Arrhenius manner and are very similar for both poly(POSS-imide)s. Differences in permeation thus stem from the diffusion coefficients. Estimates of *D* also showed Arrhenius-like behaviour with those for CO_2 being generally larger than those for CH_4 and those for the PMDA poly(POSS-imide) being in most cases larger than those in the 6FDA poly(POSS-imide). Qualitatively, the behaviour of the permeability was similar to that found experimentally [9].

While this work was carried out using a dianhydride to POSS ratio of 2:1, other cross-linking densities will have to be studied to assess the effect of this important parameter on the sorption and transport of small gases in these hybrid materials.

Acknowledgments

This work was performed within the frameworks of the Institute for Sustainable Process Technology (www.ispt.eu) and the Centre of Excellence of Multifunctional Architectured Materials "CEMAM" n° ANR-10-LABX-44-01. It was granted access to the HPC resources of CCRT/CINES/IDRIS under the allocations 2016-, 2017- and 2018-095053 made by GENCI (Grand Equipement National de Calcul Intensif), France. The MUST cluster at the University Savoie Mont Blanc (France) is also acknowledged for the provision of computer time. Nicolas Charvin is thanked for his help with the installation and maintenance of the laboratory compute servers.

Nomenclature

b	hole affinity in DMS model
$C_H^{'}$	Langmuir sorption capacity in DMS model
C_{gas}	concentration of the gas in the gas phase
C_{pol}	concentration of the gas in the polymer phase
D_i	diffusion coefficient of species i
FSV	fraction of significant volume
k_B	Boltzmann's constant
k_D	Henry's constant in DMS model
n_{gas}	number of gas molecules in the gas phase
n_{pol}	number of gas molecules in the polymer phase
$\boldsymbol{P}$	pressure tensor
p	pressure
P_i	permeability coefficient of species i
$\vec{R}_j$	vector position of the centre-of-mass of penetrant molecule j
$\left\langle \Delta R_i^2(t) \right\rangle$	mean-squared displacement of species i
S_c	solubility coefficient
S_{gas}	solubility of the gas in the gas phase
S_{pol}	solubility of the gas in the polymer phase
S_{pol}^0	infinite dilution solubility of the gas in the polymer phase
t	time
T	temperature
V	volume
α	ideal gas separation factor
ε_V	relative volume change
μ_{gas}^{ex}	excess chemical potential of the gas in the gas phase
μ_{pol}^{ex}	excess chemical potential of the gas in the polymer phase
$\Delta\Phi$	change in potential energy for the (virtual) insertion of a test particle
$\rho\left(\Delta\Phi\right)$	normalized probability density of $\Delta\Phi$
$\rho_w\left(\Delta\Phi\right)$	Boltzmann-weighted normalized probability density of $\Delta\Phi$

Notes and references

[1] C. Zhang, F. Babonneau, C. Bonhomme, R.M. Laine, C.L. Soles, H.A. Hristov, A.F. Yee, Highly Porous Polyhedral Silsesquioxane Polymers. Synthesis and Characterization, Journal of the American Chemical Society, 120 (1998) 8380-8391.

[2] C. Zhang, R.M. Laine, Hydrosilylation of Allyl Alcohol with $[HSiMe_2OSiO_{1.5}]_8$: Octa(3-hydroxypropyldimethylsiloxy)octasilsesquioxane and Its Octamethacrylate Derivative as Potential Precursors to Hybrid Nanocomposites, Journal of the American Chemical Society, 122 (2000) 6979-6988.

[3] R.M. Laine, J. Choi, I. Lee, Organic–Inorganic Nanocomposites with Completely Defined Interfacial Interactions, Advanced Materials, 13 (2001) 800-803.

[4] J. Choi, J. Harcup, A.F. Yee, Q. Zhu, R.M. Laine, Organic/Inorganic Hybrid Composites from Cubic Silsesquioxanes, Journal of the American Chemical Society, 123 (2001) 11420-11430.

[5] J. Choi, R. Tamaki, S.G. Kim, R.M. Laine, Organic/Inorganic Imide Nanocomposites from Aminophenylsilsesquioxanes, Chemistry of Materials, 15 (2003) 3365-3375.

[6] R. Tamaki, J. Choi, R.M. Laine, A Polyimide Nanocomposite from Octa(aminophenyl)silsesquioxane, Chemistry of Materials, 15 (2003) 793-797.

[7] M.Z. Asuncion, R.M. Laine, Silsesquioxane Barrier Materials, Macromolecules, 40 (2007) 555-562.

[8] I. Nischang, O. Brüggemann, I. Teasdale, Facile, Single-Step Preparation of Versatile, High-Surface-Area, Hierarchically Structured Hybrid Materials, Angewandte Chemie International Edition, 50 (2011) 4592-4596.

[9] M.J. Raaijmakers, M.A. Hempenius, P.M. Schon, G.J. Vancso, A. Nijmeijer, M. Wessling, N.E. Benes, Sieving of hot gases by hyper-cross-linked nanoscale-hybrid membranes, Journal of the American Chemical Society, 136 (2014) 330-335.

[10] M.J.T. Raaijmakers, M. Wessling, A. Nijmeijer, N.E. Benes, Hybrid polyhedral oligomeric silsesquioxanes-imides with tailored intercage spacing for sieving of hot gases, Chemistry of Materials, 26 (2014) 3660-3664.

[11] M.J.T. Raaijmakers, E.J. Kappert, A. Nijmeijer, N.E. Benes, Thermal Imidization Kinetics of Ultrathin Films of Hybrid Poly(POSS-imide)s, Macromolecules, 48 (2015) 3031-3039.

[12] M.J.T. Raaijmakers, Hyper-Cross-Linked Hybrid Membranes via Interfacial Polymerization, Ph.D. thesis, University of Twente, The Netherlands, 2015.

[13] M.J. Raaijmakers, W. Ogieglo, M. Wiese, M. Wessling, A. Nijmeijer, N.E. Benes, Sorption Behavior of Compressed CO_2 and CH_4 on Ultrathin Hybrid Poly(POSS-imide) Layers, ACS Applied Materials & Interfaces, 7 (2015) 26977-26988.

[14] D.B. Cordes, P.D. Lickiss, F. Rataboul, Recent developments in the chemistry of cubic polyhedral oligosilsesquioxanes, Chem. Rev., 110 (2010) 2081-2173.

[15] L.M. Costello, W.J. Koros, Thermally stable polyimide isomers for membrane-based gas separations at elevated temperatures, J. Polym. Sci., Part B: Polym. Phys., 33 (1995) 135-146.

[16] M. Dalwani, J. Zheng, M. Hempenius, M.J.T. Raaijmakers, C.M. Doherty, A.J. Hill, M. Wessling, N.E. Benes, Ultra-thin hybrid polyhedral silsesquioxane-polyamide films with potentially unlimited 2D dimensions, Journal of Materials Chemistry, 22 (2012) 14835-14838.

[17] K. Vanherck, G. Koeckelberghs, I.F.J. Vankelecom, Crosslinking polyimides for membrane applications: A review, Progress in Polymer Science, 38 (2013) 874-896.

[18] S. Neyertz, P. Gopalan, P. Brachet, A. Kristiansen, F. Männle, D. Brown, Oxygen transport in amino-functionalized polyhedral oligomeric silsesquioxanes (POSS), Soft Materials, 12 (2014) 113-123.

[19] S. Neyertz, D. Brown, M.J.T. Raaijmakers, N.E. Benes, A molecular characterization of hyper-cross-linked hybrid polyPOSS-imide networks, Comp. Mater. Sci., 117 (2016) 338-353.

[20] S. Neyertz, D. Brown, M.J.T. Raaijmakers, N.E. Benes, The influence of the dianhydride precursor in hyper-cross-linked hybrid polyPOSS-imide networks, Physical Chemistry Chemical Physics, 18 (2016) 28688-28703.

[21] N.F.A. van der Vegt, W.J. Briels, M. Wessling, H. Strathmann, The sorption induced glass transition in amorphous glassy polymers, The Journal of Chemical Physics, 110 (1999) 11061-11069.

[22] T. Visser, M. Wessling, When Do Sorption-Induced Relaxations in Glassy Polymers Set In?, Macromolecules, 40 (2007) 4992-5000.

[23] D. Brown, The gmq User Manual Version 5, The gmq User Manual Version 5: available at http://www.lmops.univ-savoie.fr/brown/gmq.html, (2013).

[24] G. Ciccotti, M. Ferrario, J.P. Ryckaert, Molecular dynamics of rigid systems in cartesian coordinates A general formulation, Molecular Physics, 47 (1982) 1253-1264.

[25] K.D. Hammonds, J.-P. Ryckaert, On the convergence of the SHAKE algorithm, Comput. Phys. Commun., 62 (1991) 336-351.

[26] M. Clark, R.D. Cramer, N. Van Opdenbosch, Validation of the general purpose tripos 5.2 force field, Journal of Computational Chemistry, 10 (1989) 982-1012.

[27] A.L. Frischknecht, J.G. Curro, Improved United Atom Force Field for Poly(dimethylsiloxane), Macromolecules, 36 (2003) 2122-2129.

[28] H.-C. Li, C.-Y. Lee, C. McCabe, A. Striolo, M. Neurock, Ab Initio Analysis of the Structural Properties of Alkyl-Substituted Polyhedral Oligomeric Silsesquioxanes, The Journal of Physical Chemistry A, 111 (2007) 3577-3584.

[29] R.M. Sok, H.J.C. Berendsen, W.F. van Gunsteren, Molecular dynamics simulation of the transport of small molecules across a polymer membrane, The Journal of Chemical Physics, 96 (1992) 4699-4704.

[30] A. Striolo, C. McCabe, P.T. Cummings, Thermodynamic and Transport Properties of Polyhedral Oligomeric Sislesquioxanes in Poly(dimethylsiloxane), The Journal of Physical Chemistry B, 109 (2005) 14300-14307.

[31] A. Striolo, C. McCabe, P.T. Cummings, Effective Interactions between Polyhedral Oligomeric Sislesquioxanes Dissolved in Normal Hexadecane from Molecular Simulation, Macromolecules, 38 (2005) 8950-8959.

[32] Z.A. Makrodimitri, R. Dohrn, I.G. Economou, Atomistic Simulation of Poly(dimethylsiloxane): Force Field Development, Structure, and Thermodynamic Properties of Polymer Melt and Solubility of n-Alkanes, n-Perfluoroalkanes, and Noble and Light Gases, Macromolecules, 40 (2007) 1720-1729.

[33] F.J. Feher, K.D. Wyndham, D. Soulivong, F. Nguyen, Syntheses of highly functionalized cube-octameric polyhedral oligosilsesquioxanes ($R_8Si_8O_{12}$), Journal of the Chemical Society, Dalton Transactions, (1999) 1491-1498.

[34] M.P. Allen, D.J. Tildesley, Computer Simulation of Liquids, Clarendon Press, Oxford, U.K., 1987.

[35] P.P. Ewald, Die Berechnung optischer und elektrostatisher Gitterpotentiale, Ann. Phys., 369 (1921) 253-287.

[36] W. Smith, A replicated data molecular dynamics strategy for the parallel Ewald sum, Comput. Phys. Commun., 67 (1992) 392-406.

[37] D. Brown, S. Neyertz, A general pressure tensor calculation for molecular dynamics simulations, Molecular Physics, 84 (1995) 577-595.

[38] D. Fincham, Optimisation of the Ewald sum for large systems, Mol. Simul., 13 (1994) 1-19.

[39] J. Vrabec, J. Stoll, H. Hasse, A Set of Molecular Models for Symmetric Quadrupolar Fluids, J. Phys. Chem. B, 105 (2001) 12126-12133.

[40] N. Hansen, F.A.B. Agbor, F.J. Keil, New force fields for nitrous oxide and oxygen and their application to phase equilibria simulations, Fluid Phase Equilibria, 259 (2007) 180-188.

[41] D. Yin, A.D. MacKerell, Combined ab initio/empirical approach for optimization of Lennard–Jones parameters, Journal of Computational Chemistry, 19 (1998) 334-348.

[42] I. Tanis, D. Brown, S. Neyertz, R. Heck, R. Mercier, M. Vaidya, J.-P. Ballaguet, A comparison of pure and mixed-gas permeation of nitrogen and methane in 6FDA-based polyimides as studied by molecular dynamics simulations, Computational Materials Science, 141 (2018) 243-253.

[43] Z. Zhang, Z. Duan, An optimized molecular potential for carbon dioxide, The Journal of Chemical Physics, 122 (2005) 214507.

[44] S. Pandiyan, D. Brown, S. Neyertz, N.F.A. van der Vegt, Carbon Dioxide Solubility in Three Fluorinated Polyimides Studied by Molecular Dynamics Simulations, Macromolecules, 43 (2010) 2605-2621.

[45] B. Widom, Some topics in theory of fluids, J. Chem. Phys., 39 (1963) 2808-2812.

[46] A. Ben□Naim, Y. Marcus, Solvation thermodynamics of nonionic solutes, The Journal of Chemical Physics, 81 (1984) 2016-2027.

[47] D. Frenkel, B. Smit, Understanding Molecular Simulation, Second Edition: From Algorithms to Applications (Computational Science), Academic Press, 2001.

[48] T.R. Cuthbert, N.J. Wagner, M.E. Paulaitis, Molecular Simulation of Glassy Polystyrene: Size Effects on Gas Solubilities, Macromolecules, 30 (1997) 3058-3065.

[49] G.L. Deitrick, L.E. Scriven, H.T. Davis, Efficient molecular simulation of chemical potentials, The Journal of Chemical Physics, 90 (1989) 2370-2385.

[50] G. Dömötör, R. Hentschke, Atomistically Modeling the Chemical Potential of Small Molecules in Dense Systems, The Journal of Physical Chemistry B, 108 (2004) 2413-2417.

[51] Y. Tamai, H. Tanaka, K. Nakanishi, Molecular Simulation of Permeation of Small Penetrants through Membranes. 2. Solubilities, Macromolecules, 28 (1995) 2544-2554.

[52] L. Cui, W. Qiu, D.R. Paul, W.J. Koros, Physical aging of 6FDA-based polyimide membranes monitored by gas permeability, Polymer, 52 (2011) 3374-3380.

[53] J.H. Kim, W.J. Koros, D.R. Paul, Physical aging of thin 6FDA-based polyimide membranes containing carboxyl acid groups. Part I. Transport properties, Polymer, 47 (2006) 3094-3103.

[54] W.-H. Lin, T.-S. Chung, Gas permeability, diffusivity, solubility, and aging characteristics of 6FDA-durene polyimide membranes, Journal of Membrane Science, 186 (2001) 183-193.

[55] J.H. Kim, W.J. Koros, D.R. Paul, Physical aging of thin 6FDA-based polyimide membranes containing carboxyl acid groups. Part II. Optical properties, Polymer, 47 (2006) 3104-3111.

[56] M.R. Coleman, W.J. Koros, Conditioning of Fluorine Containing Polyimides. 1. Effect of Exposure to High Pressure Carbon Dioxide on Permeability, Macromolecules, 30 (1997) 6899-6905.

[57] M.R. Coleman, W.J. Koros, Conditioning of Fluorine-Containing Polyimides. 2. Effect of Conditioning Protocol at 8 Volume Dilation on Gas-Transport Properties, Macromolecules, 32 (1999) 3106-3113.

[58] C. Fuhrman, M. Nutt, K. Vichtovonga, M.R. Coleman, Effect of thermal hysteresis on the gas permeation properties of 6FDA□based polyimides, Journal of Applied Polymer Science, 91 (2003) 1174-1182.

[59] J.D. Wind, C. Staudt-Bickel, D.R. Paul, W.J. Koros, Solid-State Covalent Cross-Linking of Polyimide Membranes for Carbon Dioxide Plasticization Reduction, Macromolecules, 36 (2003) 1882-1888.

[60] S. Neyertz, D. Brown, Nanosecond-time-scale reversibility of dilation induced by carbon dioxide sorption in glassy polymer membranes, Journal of Membrane Science, 520 (2016) 385-399.

[61] R. Paterson, Y. Yampol'skii, P.G.T. Fogg, A. Bokarev, V. Bondar, O. Ilinich, S. Shishatskii, IUPAC-NIST Solubility Data Series 70. Solubility of Gases in Glassy Polymers, Journal of Physical and Chemical Reference Data, 28 (1999) 1255-1450.

[62] Y.P. Yampolskii, I. Pinnau, B.D. Freeman, Materials Science of Membranes for Gas and Vapour Separation, John Wiley & Sons Ltd, 2006.

[63] P.V.K. Pant, R.H. Boyd, Molecular dynamics simulation of diffusion of small penetrants in polymers, Macromolecules, 26 (1993) 679-686.

[64] S. Neyertz, D. Brown, Molecular dynamics study of carbon dioxide sorption and plasticization at the interface of a glassy polymer membrane, Macromolecules, 46 (2013) 2433-2449.

[65] S. Neyertz, D. Brown, The effect of structural isomerism on carbon dioxide sorption and plasticization at the interface of a glassy polymer membrane, Journal of Membrane Science, 460 (2014) 213-228.

[66] L.M. Robeson, Z.P. Smith, B.D. Freeman, D.R. Paul, Contributions of diffusion and solubility selectivity to the upper bound analysis for glassy gas separation membranes, Journal of Membrane Science, 453 (2014) 71-83.

[67] M.K. Ghosh, K.L. Mittal, Polyimides: Fundamentals and Applications, in, Marcel Dekker, Inc., New York, 1996.

[68] D. Brown, V. Marcadon, P. Mélé, N.D. Albérola, Effect of Filler Particle Size on the Properties of Model Nanocomposites, Macromolecules, 41 (2008) 1499-1511.

[69] V.I. Bondar, Y. Kamiya, Y.P. Yampol'skii, On pressure dependence of the parameters of the dual-mode sorption model, Journal of Polymer Science Part B: Polymer Physics, 34 (1996) 369-378.

[70] R. Kirchheim, Sorption and partial molar volume of small molecules in glassy polymers, Macromolecules, 25 (1992) 6952-6960.

[71] D.N. Bol'shutkin, V.M. Gasan, A.I. Prokhvatilov, Temperature dependence of the crystalline lattice parameter of methane in the range of 11–70°K, Journal of Structural Chemistry, 12 (1971) 670-672.

[72] V.G. Manzhelii, A.M. Tolkachev, M.I. Bagatskii, E.I. Voitovich, Thermal expansion, heat capacity, and compressibility of solid CO2, Physica Status Solidi (b), 44 (1971) 39-49.

[73] F. Müller-Plathe, Calculation of the free energy for gas absorption in amorphous polypropylene, Macromolecules, 24 (1991) 6475-6479.

[74] E. Saiz, M.M. Lopez Gonzalez, E. Riande, J. Guzman, V. Compan, Simulations of diffusive and sorption processes of gases in polyimide membranes: Comparison with experiments, Physical Chemistry Chemical Physics, 5 (2003) 2862-2868.

[75] M. Heuchel, D. Hofmann, P. Pullumbi, Molecular Modeling of Small-Molecule Permeation in Polyimides and Its Correlation to Free-Volume Distributions, Macromolecules, 37 (2004) 201-214.

[76] P.H. Pfromm, The Impact of Physical Aging of Amorphous Glassy Polymers on Gas Separation Membranes, in: Y.P. Yampolskii, I. Pinnau, B.D. Freeman (Eds.) Materials Science of Membranes for Gas and Vapour Separation, John Wiley & Sons Ltd., Hoboken, N.J., USA, 2006.

[77] M. Böhning, J. Springer, Sorptive dilation and relaxational processes in glassy polymer/gas systems—I. Poly(sulfone) and poly(ether sulfone), Polymer, 39 (1998) 5183-5195.

[78] D.S. Pope, G.K. Fleming, W.J. Koros, Effect of various exposure histories on sorption and dilation in a family of polycarbonates, Macromolecules, 23 (1990) 2988-2994.

[79] T.-S. Chung, S.S. Chan, R. Wang, Z. Lu, C. He, Characterization of permeability and sorption in Matrimid/C60 mixed matrix membranes, Journal of Membrane Science, 211 (2003) 91-99.

[80] A. Scholes Colin, X. Tao Wen, W. Stevens Geoff, E. Kentish Sandra, Sorption of methane, nitrogen, carbon dioxide, and water in Matrimid 5218, Journal of Applied Polymer Science, 117 (2010) 2284-2289.

[81] J.D. Wind, Improving Polyimide Membrane Resistance to Carbon Dioxide Plasticization in Natural Gas Separations, Ph.D thesis, University of Texas, 2002.

[82] F. Müller-Plathe, Permeation of polymers — a computational approach, Acta Polymerica, 45 (1994) 259-293.

[83] A.A. Gusev, F. Müller-Plathe, W.F. van Gunsteren, U.W. Suter, Dynamics of small molecules in bulk polymers, in: L. Monnerie, U.W. Suter (Eds.) Atomistic Modeling of Physical Properties, Springer Berlin Heidelberg, Berlin, Heidelberg, 1994, pp. 207-247.

[84] M.L. Greenfield, D.N. Theodorou, Molecular Modeling of Methane Diffusion in Glassy Atactic Polypropylene via Multidimensional Transition State Theory, Macromolecules, 31 (1998) 7068-7090.

[85] S. Neyertz, Gas transport in dense polymeric membranes, molecular dynamics simulations, in: E.M.V. Hoek, V.V. Tarabara (Eds.) Encyclopedia of Membrane Science and Technology, John Wiley & Sons, Hoboken, NJ, 2013.

[86] S. Neyertz, D. Brown, S. Pandiyan, N.F.A. van der Vegt, Carbon Dioxide Diffusion and Plasticization in Fluorinated Polyimides, Macromolecules, 43 (2010) 7813-7827.

[87] S. Neyertz, D. Brown, A Trajectory-Extending Kinetic Monte Carlo (TEKMC) Method for Estimating Penetrant Diffusion Coefficients in Molecular Dynamics Simulations of Glassy Polymers, Macromolecules, 43 (2010) 9210-9214.

[88] W. Humphrey, A. Dalke, K. Schulten, VMD: visual molecular dynamics, J. Mol. Graphics, 14 (1996) 33-38.